

P-907: Proposal to Measure Particle Production in the Meson Area Using Main Injector Primary and Secondary Beams

May 2000

Y. Fisyak,
Brookhaven National Laboratory

A. Godley, S.R. Mishra, C. Rosenfeld,
University of South Carolina

R. Winston,
Enrico Fermi Institute, University of Chicago

E. Swallow,
Elmhurst College and EFI

J. Hylen, N. Mokhov, J. Morfin, C.T. Murphy, A. Para, R. Raja,¹ S. Striganov,
Fermi National Accelerator Laboratory

M. Messier,
Harvard University

D. Asner, P.D. Barnes, Jr., D. Fujino, E. Hartouni, S. Johnson, R. Soltz, D. Wright,
C. Wuest,
Lawrence Livermore National Laboratory

B. Cole,
Nevis Laboratories

L. Gutay,
Purdue University

S. Chernichenko, Y. Galitsky, Y. Gutnikov, V. Onuchin, E. Melnikov, V. Semenov,
IHEP, Protvino

S. Wojcicki,
Stanford University

¹Spokesperson

Abstract

We propose to measure hadronic particle production with excellent particle identification using primary and secondary beams from the Main Injector. The goals of the experiment are: to verify a general scaling law of hadronic fragmentation; to measure particle production off NuMI targets using 120 GeV/ c protons with sufficient accuracy to predict the NuMI neutrino spectrum; and to collect a comprehensive data set that would have a profound impact on related physics issues, such as atmospheric neutrino flux estimates, neutrino factory design, and simulations of hadronic showers for high-energy colliders. This experiment could also form the basis for a long-term program in light-meson spectroscopy.

Contents

1	Executive Summary	1
2	Introduction	2
3	Physics Motivation	4
3.1	Scaling Law of Hadronic Fragmentation	4
3.2	Systematic Errors in NuMI/MINOS Measurements of Neutrino Oscillation Parameters	7
3.3	Preliminary Study on Sensitivity of Neutrino Oscillation Parameters to Spectral Variations in MINOS	9
3.4	Proton-Nucleus Physics	17
3.5	Measurements for Atmospheric Neutrino Physics	24
3.6	Neutrino Factory Needs	25
3.7	Quality of Existing Hadroproduction Data	25
3.8	Light Meson Spectroscopy	28
4	Beam and Experimental Layout	31
4.1	Implementation Scheme	31
4.2	Beam Requirements	32
4.3	Event Rates	34
4.4	Primary Beam Rate Requirements	37
4.5	Running Time Requirements	38
5	Detector Performance	41
5.1	Particle Acceptances	41
5.2	Particle Resolutions	41
5.3	Particle Identification	41
5.4	Data Acquisition	45
6	Cost and Schedule	48
6.1	Cost Estimate	48
6.1.1	Scope of Estimate	48
6.1.2	Estimate Methodology and Basis	49
6.1.3	Contingency	53
6.2	Manpower Estimate	54
6.2.1	Physicist Effort for Core Analysis	54
A	Schedule for 120 GeV Beam to the Meson Lab	56
	References	57

1 Executive Summary

We propose a low-cost experiment, P-907, using existing hardware, to measure particle production off hydrogen, a variety of nuclei and the NuMI targets, with excellent particle identification. The quality of data thus obtained will be a significant improvement over existing measurements. The data obtained will be used:

- To explore the accuracy with which a general scaling law of fragmentation is valid over a range of energy and particle type.
- To measure particle production off NuMI targets with sufficient accuracy to predict the neutrino spectra at the near and far detectors in MINOS, with and without the presence of the “hadronic hose.”
- To provide a starting point for the study of the dynamics of non-perturbative QCD and its associated resonances.
- To gain a better understanding of the propagation of particles in nuclei.
- To improve predictions of atmospheric neutrino fluxes.
- To design accelerator neutrino factories.
- To improve hadronic shower models in collider simulation programs such as Geant.

A key feature of this experiment is the high-precision identification of the produced particle species across the entire kinematic range accessible with primary beam from the Main Injector. This is crucial to accomplish the goals stated above. We achieve nearly complete particle identification for π , K , and p from 0.1–80 GeV/ c by measuring: energy loss in a TPC, threshold Čerenkov radiation, time of flight, and ring-imaged Čerenkov radiation.

We propose to spend most of our running time in a survey mode. The secondary beamline we propose for Meson Center will allow us to acquire data at one rigidity for π , K , and p of one charge sign simultaneously. The incident secondary beam species will be tagged by threshold Čerenkov counters before the 1% interaction length experimental target. In 126 hours of running we can acquire one million events for each incident species. We plan to scan the momentum range 5–110 GeV/ c and use a set of experimental targets spanning the periodic table, from hydrogen to lead.

We also propose to acquire data using 120 GeV/ c Main Injector primary beam directly onto the NuMI targets. In approximately 90 hours we can measure the spectrum of produced π ’s to 1% across the entire range relevant for NuMI, 1–50 GeV/ c . Since K ’s are produced at approximately 10% of the rate for π ’s, and both are produced with a fairly flat longitudinal spectrum, particle identification across this entire range is crucial for the measurement. Despite the apparently short running time required, an experiment of this size is required to obtain the required particle identification capability.

2 Introduction

We propose to make a set of measurements of hadron-nucleus interactions as a function of beam momentum, to extend the ability to predict the behavior of “minimum bias” events occurring at high cross section (99% of the inelastic cross section). The ability to predict particle production from these reactions is based on a number of empirical relationships which form various computational models widely employed by the High Energy Physics community (e.g. FLUKA, MARS, etc). For the most part, the empirical relationships are derived from data taken in the 1960’s and 1970’s from a wide variety of experiments spanning a range of beam species, target nuclei and energy. This legacy data has many gaps and some results from different experiments disagree significantly.

While these models of particle production have been used successfully for a couple of decades, a series of important physics issues have recently pushed beyond the limits of applicability for the models. It has been realized in the design stages of a $\mu\mu$ collider that the uncertainties in the pion production spectrum introduce large uncertainties in our ability to calculate source yield, and hence the luminosity of such a facility. A related physics issue of great importance to understanding fundamental physics questions is the inability to predict pion and kaon production, resulting in uncertainties in calculations of neutrino yields. The ability to calculate neutrino yields from hadron-nucleus interactions affects the interpretation of current experimental observations, and planning and analysis for future neutrino experiments. A recent neutrino experiment at CERN, NOMAD, required neutrino production data at a level beyond the capability of current production models and motivated the SPY [11] experiment, also at CERN, to collect that data.

The focus of this experiment is to provide data on “minimum bias” events as the basis of the next generation of production models. A general “survey” approach (generating a data set in beam species, target nuclei, and beam momentum space) will be directed to providing data for various models of particle production, *e.g.*, investigating scaling laws, extending ideas in pA physics, verifying and validating production models. The apparatus used to collect this data can also be used to answer specific questions of particle production necessary for understanding neutrino production, as is required for the Fermilab NuMI project in the analysis of the MINOS measurement of neutrino oscillations.

The development of HEP detector technology of the 1980’s and 1990’s in multi-particle spectrometers will be utilized to assemble an apparatus capable of generating a large, well measured data sample in a reasonable running time.

The center-piece of the experiment is the EOS Time Projection Chamber (TPC), built by the BEVALAC group[1] at Lawrence Berkeley National Laboratory and, until recently, part of the E-910 experiment at Brookhaven National Laboratory. The ownership of the TPC has been transferred from LBNL to Fermilab and the TPC has been transported to Fermilab, complete with its electronics and data acquisition hardware. The software for reconstruction and simulation of the TPC has taken many years of development and is quite sophisticated and is available for our experiment. The TPC is currently capable of taking data at $\approx 60\text{Hz}$ and we believe we can upgrade the electronics to acquire data at $\approx 100\text{Hz}$.

Another important component is the SELEX Ring imaging Čerenkov counter (RICH) that performed wonderfully for the SELEX experiment[2]. It enables the separation of pions, kaons and protons to momenta exceeding 120 GeV/c and provides particle identification

capabilities in the very forward region. The simulation and reconstruction software for the SELEX RICH is also in hand.

This is a more detailed version of the proposal we submitted to the PAC in March 1999. We have expanded each of the sections and have included a detailed cost analysis in section 6. In section 3 we motivate each of the aims of the experiment. In section 4 we describe the layout of the apparatus and estimate the expected event rates. In section 5 we detail the apparatus acceptance, resolution, particles identification efficiencies, and the data acquisition system performance.

3 Physics Motivation

3.1 Scaling Law of Hadronic Fragmentation

Even though they form more than 90% of the total inelastic cross section, very little is known about the dynamics of minimum bias interactions. The events are of such low Q^2 that perturbative QCD has little predictive power. Several scaling laws, such as KNO scaling and Feynman scaling, have in the past been proposed to explain the dynamics of minimum bias interactions. All of these have been shown to disagree with experiment.

In 1978, a general law of scaling for inclusive reactions was proposed [15]. It was deduced heuristically, from the need to treat charged pions on an equal footing with neutral pions when extracting the annihilation cross sections, by considering the difference between $\bar{p}p$ and pp cross sections. There were two Phys. Rev. D papers [16][15]. The first shows that it is possible to estimate the annihilation component of $\bar{p}p \rightarrow \pi^0$ inclusive reactions by subtracting the corresponding $pp \rightarrow \pi^0$ component. However, this method fails for the channels $\bar{p}p \rightarrow \pi^+/\pi^-$ because of the different CP symmetry of the corresponding pp component. The situation is remedied by postulating a new equation involving charge asymmetry in $\bar{p}p$ annihilation and non-annihilation components. The new equation lets us extract annihilation information for charged as well as neutral pions by comparing $\bar{p}p$ and pp reactions. These equations were shown to work for 12 GeV/c annihilation reactions.

The scaling law in question was proposed in order to explain the physics behind the asymmetry equation. It states that the ratio of a semi-inclusive cross section to an inclusive cross section involving the same particles is a function only of the missing mass squared (M^2) of the system and not of the other two Mandelstam variables s and t , the center of mass energy squared and the momentum transfer squared, respectively.

Stated mathematically, the ratio

$$\frac{f_{subset}(a+b \rightarrow c+X)}{f(a+b \rightarrow c+X)} \equiv \frac{f_{subset}(M^2, s, t)}{f(M^2, s, t)} = \beta_{subset}(M^2) \quad (1)$$

i.e., a ratio of two functions of three variables is only a function of one of them. When the subset being considered is annihilations, the asymmetry equation derived in [16] results. The physics behind the scaling law may be understood [15] by considering inclusive cross sections as the analytic continuations of crossed three body interactions, which factorize into a production term that results in the formation of a shortlived fireball of mass M^2 , which subsequently decays into the subset in question. The formation is governed by s and t . The decay term is only a function of M^2 . It should be noted that the physics in question falls outside the scope of perturbative QCD and as such the scaling law is not currently derivable from QCD considerations.

The law was verified in 100 GeV $\bar{p}p$ interactions by considering multiplicity subsets of the reaction $\bar{p}p \rightarrow \pi + X$. It was possible to verify the t independence of the ratio β_{subset} for a variety of subsets with an excellent degree of accuracy. The paper [15] also establishes the s independence of β_{subset} for a variety of $pp \rightarrow p + X$ reactions in the beam energy range of 200–400 GeV/c. Again, good agreement was obtained between the predictions of the law and data. Recently, the law has been verified in 12 reactions using data from the European Hybrid Spectrometer[17] with various beam particles and final states. Figures 1 and 2 show

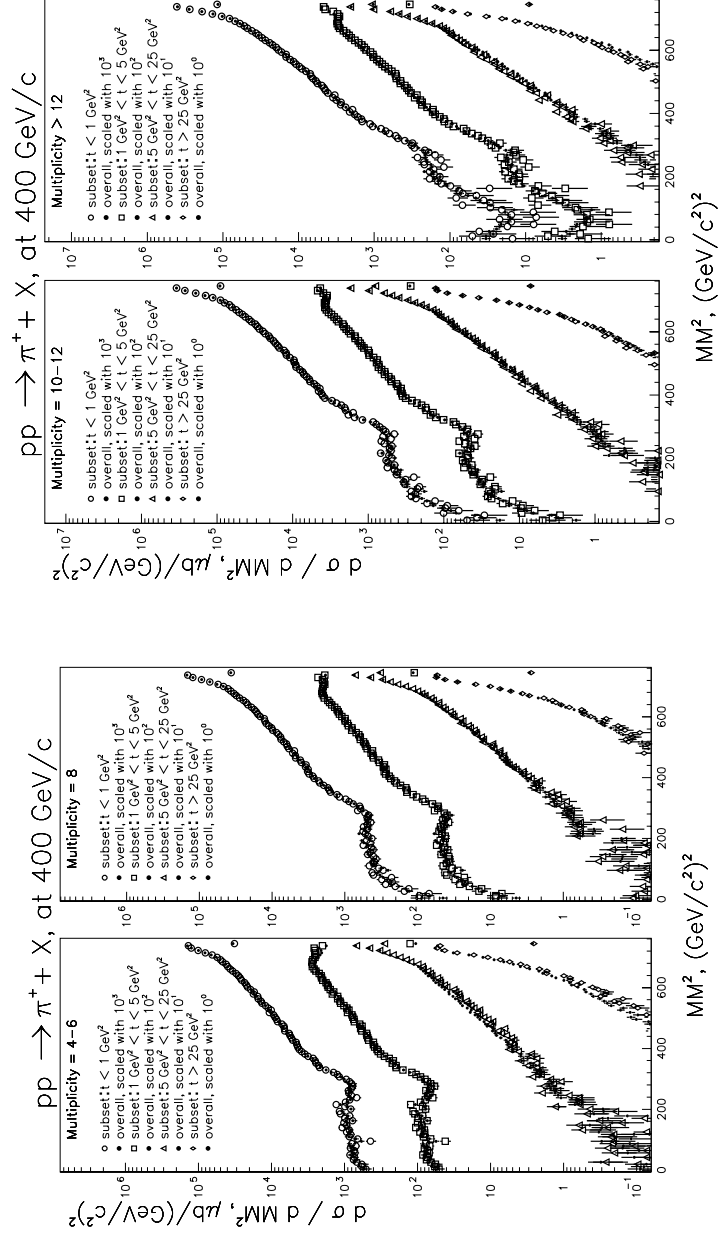


Figure 1: M^2 distribution for the various subsets in various t ranges. Overall data, weighted by appropriate $\beta_{subset}(M^2)$ is superimposed on the subset data. Data for each t range is offset from the neighboring one by a factor of 10.

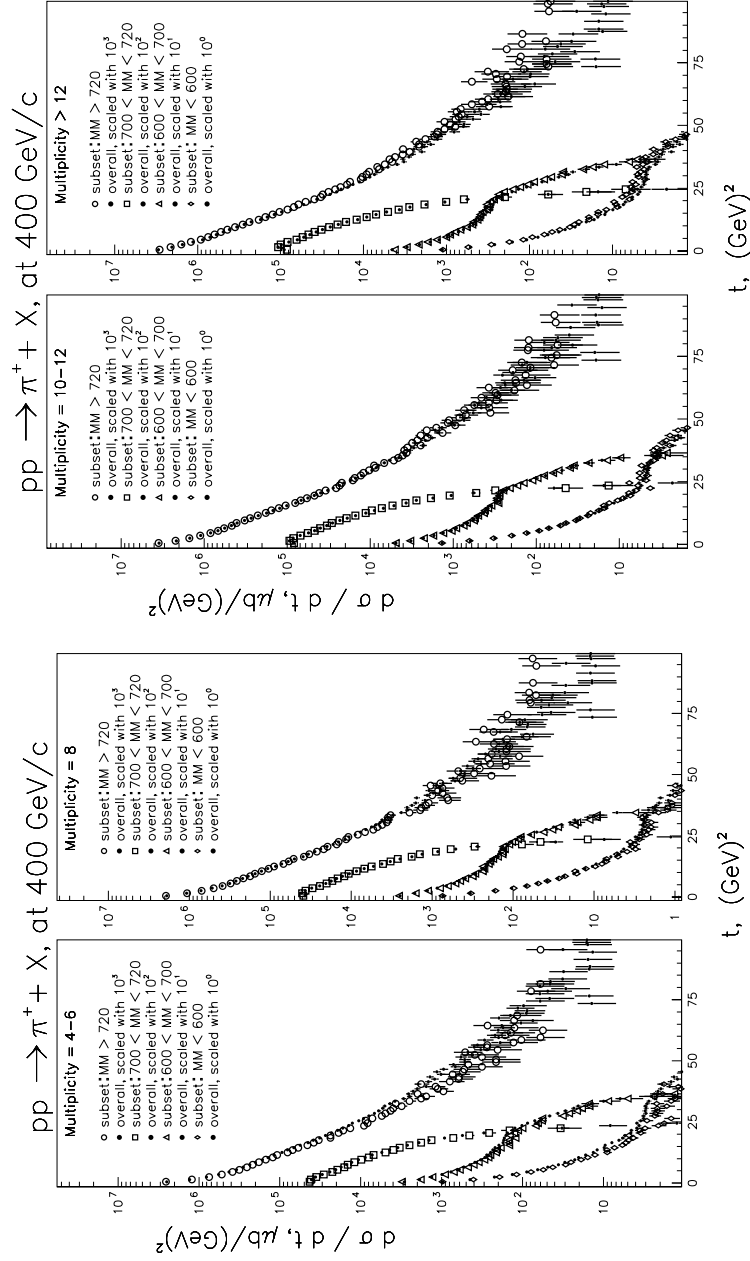


Figure 2: t distribution for the various subsets in various M^2 ranges. Overall data, weighted by appropriate $\beta_{subset}(M^2)$ is superimposed on the subset data. Data for each M^2 range is offset from the neighboring one by a factor of 10.

the test of the law for the reaction $pp \rightarrow \pi^+ + X$ for 400 GeV/ c proton beam for 4 multiplicity subsets: 4-6 prongs, 8 prongs, 10-12 prongs and >12 prongs. Figure 1 shows the agreement between the predictions of the scaling law and subset data as a function of M^2 for various t ranges. Figure 2 shows the agreement between the predictions of the scaling law and subset data as a function of t for various M^2 ranges. The agreement between the predictions of the scaling law and data is excellent in the data tested so far. If the law is an exact one, as there is reason to believe it may be, then it is clearly of fundamental importance in understanding hadronic fragmentation.

The problem with existing data is that it is usually sparse as bubble chambers were being used. *It is very difficult to test the law using existing data for s independence, since only rarely has the same apparatus been used to study the same reaction at multiple energies.*

We propose to measure particle production off hydrogen and other targets as a function of beam energy for various secondary beams ($\pi^\pm, K^\pm, p, \bar{p}$), for a variety of beam momenta ranging from 5 GeV/ c to 120 GeV/ c . At each beam momentum, the data taking rate has to be such that approximately a million unbiased events are recorded for analysis.

3.2 Systematic Errors in NuMI/MINOS Measurements of Neutrino Oscillation Parameters

One of the methods for measuring neutrino oscillation parameters (i.e., neutrino generation mass differences and mixing angles) in the MINOS experiment is to observe a distortion in the neutrino energy spectrum observed in the “far” detector located in the Soudan mine in Minnesota. To observe such a distortion it is necessary to be able to predict with good precision the shape of the neutrino energy spectrum at Soudan in the absence of oscillations. This is done through a combination of measuring the spectrum at a “near” detector (on the Fermilab site) in concert with various NuMI beam monitoring measurements.

Monte Carlo studies have shown that the largest contributor to the systematic error in the prediction of the shape of the neutrino energy spectrum at the far detector is the uncertainty in the production spectra at the target. That is, the uncertainties in the p_T and x_F distributions of the pions and kaons produced in the target (as well as their relative production rates) cannot be compensated by measurements made in the near detector. This is because the near detector makes a measurement of the neutrino energy spectrum only, whereas the particle spectra at the target are a function of two variables, the Feynman x_f and the p_t of each particle. The near detector measurements are not sufficient to fully constrain the functional variations, and particle production data at the target are needed. The experimental data to date on these spectra have very large statistical and systematic errors (on the order of 20%, see section 3.7). MINOS would greatly benefit from precise experimental data on these production spectra.

In addition, an accurate production spectra within the NuMI Beam Monte Carlo (GNuMI) at beam startup will greatly facilitate understanding and aid in the commissioning of the neutrino beam. Without knowledge of the production spectra it is very difficult to determine if large differences between expected and measured distributions of hadrons and muons at beam monitoring stations and, eventually, ν events in the near detector, are due to incorrect input hadron spectra or problems with one or more of the beam line elements

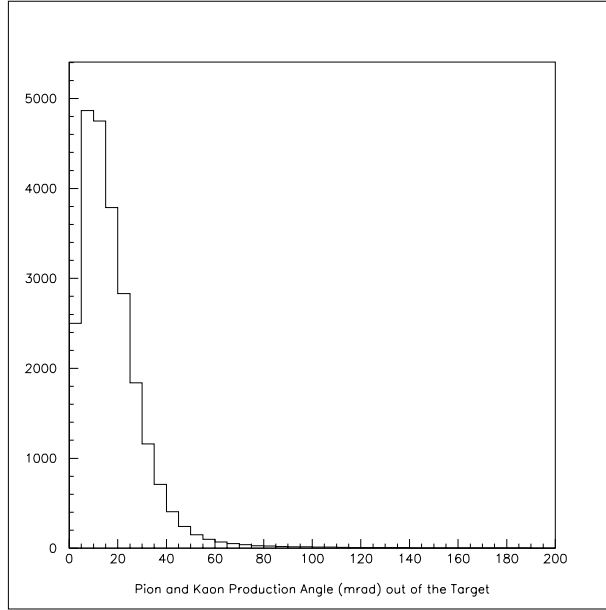


Figure 3: The hadron production angle out of the target for NuMI.

(*e.g.* target and horns).

In order to address the physics phase space relevant to NuMI, the following conditions must be met:

- The beam must be 120 GeV/ c protons with a phase space similar to that of the Main Injector.
- The targets must be the same as the NuMI targets, “fin” targets (i.e., rectangular in shape), approximately 0.94 m (low energy beam option) or 1.42 m (medium energy beam option) in length and 3.2 mm thick.
- The p_T and x_F (or just momentum) distributions must be measured to a precision of around 2%.
- The target exit point of the hadrons must be measured.
- Particle identification must be performed for hadrons with momentum from 5 to 80 GeV/ c . Identification for hadrons up to 100 GeV/ c would be useful but is not crucial.
- The forward acceptance must be at least 100 mrad (see Figure 3).
- K_S^0 production must be measured. Presumably the p and p_T distributions can be measured using the $K_S^0 \rightarrow \pi^+ \pi^-$ decay channel, although the exit point resolution will probably not be good enough to give useful information.

To make the measurement as Monte-Carlo independent as possible, minimizing reabsorption and cascade effects, the production measurement should be done with the actual NuMI target.

A large number of highly forward protons are expected, comparable to the number of pions at high momentum. It is very important to have particle identification to statistically separate these protons from the pion yield. Because the neutrino production from kaons and pions is very different, particle identification to statistically separate these species is also important.

3.3 Preliminary Study on Sensitivity of Neutrino Oscillation Parameters to Spectral Variations in MINOS

In the following, we show a preliminary attempt to quantify the sensitivity of neutrino oscillation parameters, δm_{32}^2 and $\sin^2 2\theta_{23}$, to changes in the neutrino spectrum. We emphasize that this is a very involved problem; a complete study is currently underway in the MINOS collaboration with full results expected in a few months.

The calculation of the MINOS near and far spectra are made using a GEANT-based simulation of the NuMI beamline coupled with a simulation of neutrino-iron interactions. These programs (GNuMI and NEUGEN) are currently in use by the NuMI/MINOS collaboration for calculation of expected neutrino rates and spectra.

The expected reconstructed neutrino spectra in the MINOS near and far detector are estimated by applying reconstruction efficiencies and energy resolutions at the vector level. The reconstructed neutrino energy is taken as $E_\nu = P_\mu + E_H$ where E_ν is the reconstructed neutrino energy, P_μ is the reconstructed muon momentum and E_H is the reconstructed hadronic shower energy. Following the MINOS Technical Design Report, the resolution of P_μ is taken to be 12%, and the resolution of E_H is taken to be $(7 + 60/\sqrt{E_H[\text{GeV}]})\%$ [48]. The reconstruction efficiency for ν_μ charged-current events is taken to be $2/(e^{-3P_\mu[\text{GeV}]} + 1.0) - 1$, which is comparable to estimates used in other MINOS studies. The probability for a neutral-current event to be mis-identified as a ν_μ charged-current event is taken to be $0.5e^{-0.5(E_H)[\text{GeV}]} + 0.01$. Data quality cuts are assumed to reduce the data by 50%, consistent with other MINOS studies.

The simulation of the NuMI beamline uses the GEANT version of FLUKA (“GFLUKA”) to model hadronic production. This model produces pions with a mean p_T of 0.37 GeV. This is one of many models of hadronic production. Other models predict $\langle p_T \rangle$ values of 0.42 GeV (WANG [49]), 0.44 GeV (CKP [50]), and 0.5 GeV (Malensek [51]). (Note that none of these models include the recently measured p_\perp - x_F correlations which seem to be significant in the p_\perp , x_F range of the MINOS experiment). To cover this range of $\langle p_T \rangle$ predictions we introduced a simple warping of the hadron p_T spectrum which changes the mean p_T value for the GFLUKA model from 0.37 GeV to 0.55 GeV. This simple warping factor does not account for variations in the x_F distributions of the hadrons, which may also be significant. The warping is adequate, however, to gauge the sensitivity of the MINOS near and far spectra to changes in the hadronic production model. More detailed studies are in progress.

Figure 4 shows the distribution of the measured energy of neutrinos, E_ν , at the far detector of a 10 kiloton-year run of the low energy beam option of the MINOS experiment for (a) the Geant Fluka particle production model and (b) for the modified spectrum model. E_ν is defined as the sum of the measured muon energy and the hadronic energy. The various

sets of curves are for $\sin^2 2\theta_{23} = 1.0$ and $\delta m_{32}^2 = 0.0, 0.001, 0.002, \dots 0.007 \text{ eV}^2$.

Figure 5 shows the corresponding distributions for the MINOS medium energy beam.

Using the curves in Figures 4 and 5, it is possible to generate theoretical spectra for any value of $\sin^2 2\theta_{23}$ and δm_{32}^2 . For extrapolating in $\sin^2 2\theta_{23}$, we use the fact that events missing due to oscillation are proportional to $\sin^2 2\theta_{23}$. Extrapolation in δm_{32}^2 is done in the histograms bin by bin with polynomial interpolation using the method of divided differences. The method is described in [52]. Experimental histograms are generated from theoretically expected curves using random numbers. Fitting is done using unbinned likelihoods by the minimizing program MINUIT.

Figure 6 shows the 90% CL contours for a 10 kiloton-year MINOS low energy beam run for $\sin^2 2\theta_{23} = 0.8$ and $\delta m_{32}^2 = 0.003 \text{ eV}^2$, for the four cases (a) Geant Fluka used for both theory and experiment, (b) Geant Fluka used for theory and modified spectrum for experiment, (c) modified spectrum used for theory and experiment and (d) modified spectrum used for theory and Geant Fluka used for experiment. Within statistics, the generated and fitted values should agree for (a) and (c). The extent to which there is disagreement in (b) and (d) between the fitted and generated values shows the sensitivity of the result to assumptions of particle production spectra. Figure 7 shows the experimentally generated points (histograms with error bars) and the fitted curves (hatched histograms) for the four cases (a), (b), (c) and (d) described above.

Figure 8 shows the 90% CL contours for a 10 kiloton-year MINOS medium energy beam run for $\sin^2 2\theta_{23} = 0.8$ and $\delta m_{32}^2 = 0.005 \text{ eV}^2$, for the four cases (a) Geant Fluka used for both theory and experiment, (b) Geant Fluka used for theory and modified spectrum for experiment, (c) modified spectrum used for theory and experiment and (d) modified spectrum used for theory and Geant Fluka used for experiment. Within statistics, the generated and fitted values should agree for (a) and (c). The extent to which there is disagreement in (b) and (d) between the fitted and generated values shows the sensitivity of the result to assumptions of particle production spectra. Figure 9 shows the experimentally generated points (histograms with error bars) and the fitted curves (hatched histograms) for the four cases (a), (b), (c) and (d) described above.

We have shown that distortions in production spectra do lead to systematic errors in estimating the oscillation parameters. It is beyond the scope of this proposal to estimate how well the far detector spectra can be estimated using the near detector observed spectra. Such results should be available once the ongoing study within the MINOS collaboration comes to a conclusion. What we have shown here are examples that give an indication of how sensitive the estimation of the oscillation parameters is to distortions in the spectra. In general, the distortions in particle production are functions of both the Feynman x_f and p_t of the particle. It is functionally possible to introduce correlations between x_f and p_t such that the information contained in the near detector energy spectrum alone is insufficient to constrain the problem completely, since the near detector and the far detector sample different regions of x_f and p_t . A further complication arises from multiple interactions in the target, in that the errors in the particle production codes get compounded as the shower proceeds in the target. While it may well be possible to unfold the particle production spectra using the near detector alone for some set of correlation assumptions, we wish to point out that the analysis of both the near and far detector data, with the detector resolution effects, trigger threshold effects and acceptances is much simplified if the particle production

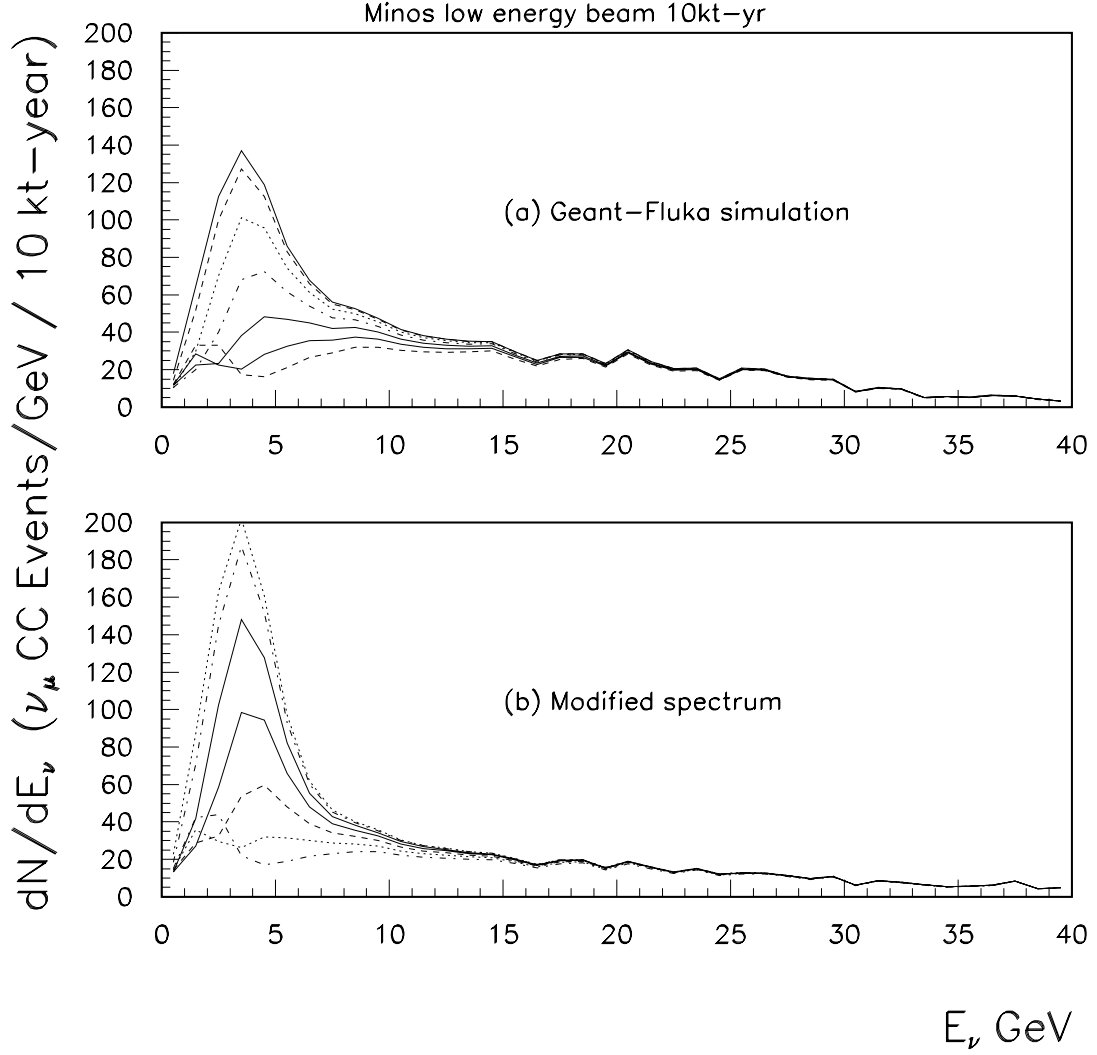


Figure 4: MINOS low energy beam spectra expected at the far detector for $\delta m_{32}^2 = 0.0, 0.001, 0.002, 0.003, 0.004, 0.005, 0.006, 0.007 \text{ eV}^2$. The curve with the largest number of events is the one for no-oscillations, *i.e.*, $\delta m_{32}^2 = 0.0$. The curve with the least number of events corresponds to $\delta m_{32}^2 = 0.007 \text{ eV}^2$. Panel (a) is for the Geant Fluka model of hadronic spectra and (b) for the modified spectrum.

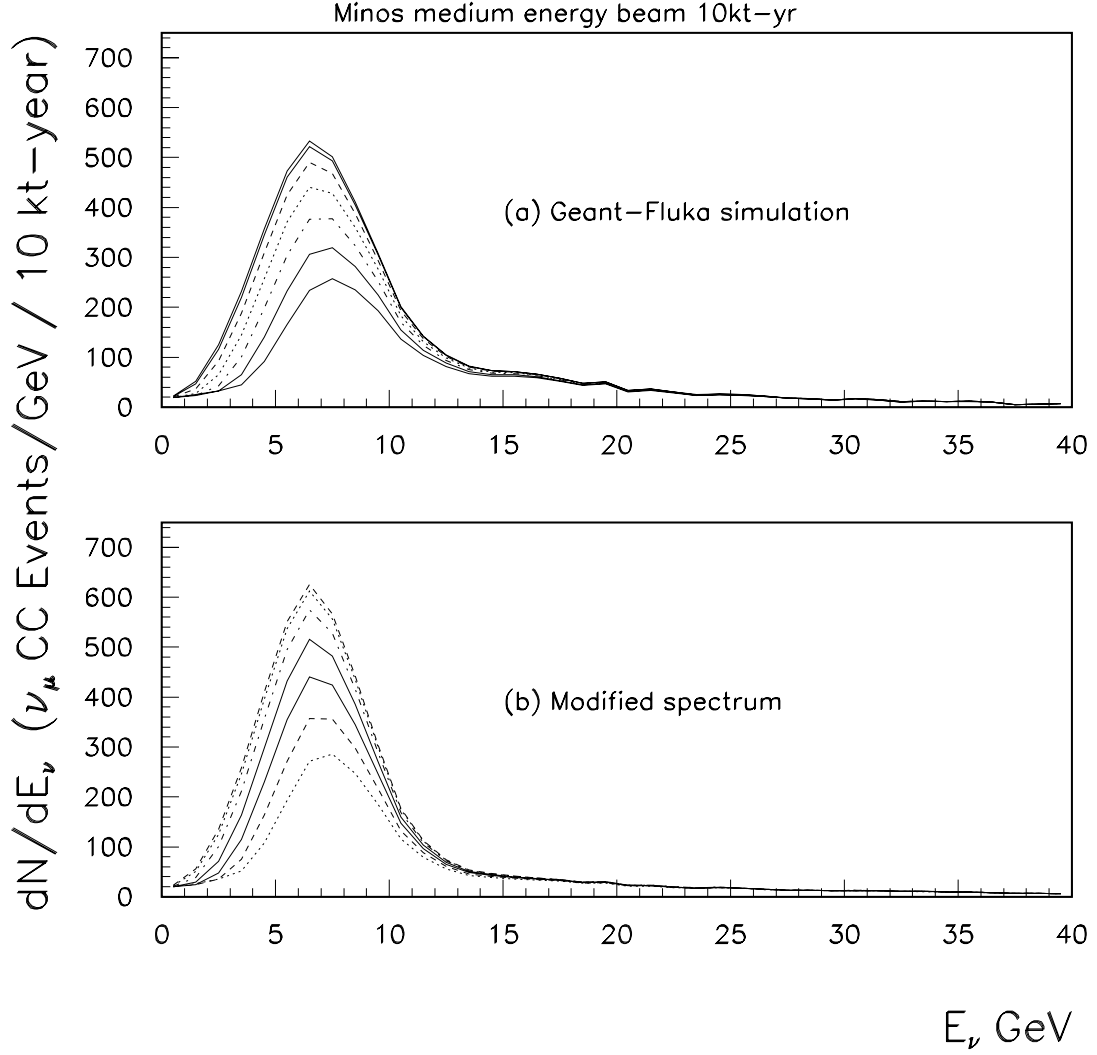


Figure 5: MINOS medium energy beam spectra expected at the far detector for $\delta m_{32}^2 = 0.0, 0.001, 0.002, 0.003, 0.004, 0.005, 0.006, 0.007$ eV². The curve with the largest number of events is the one for no-oscillations, *i.e.*, $\delta m_{32}^2 = 0.0$. The curve with the least number of events corresponds to $\delta m_{32}^2 = 0.007$ eV². Panel (a) is for the Geant Fluka model of hadronic spectra and (b) for the modified spectrum.

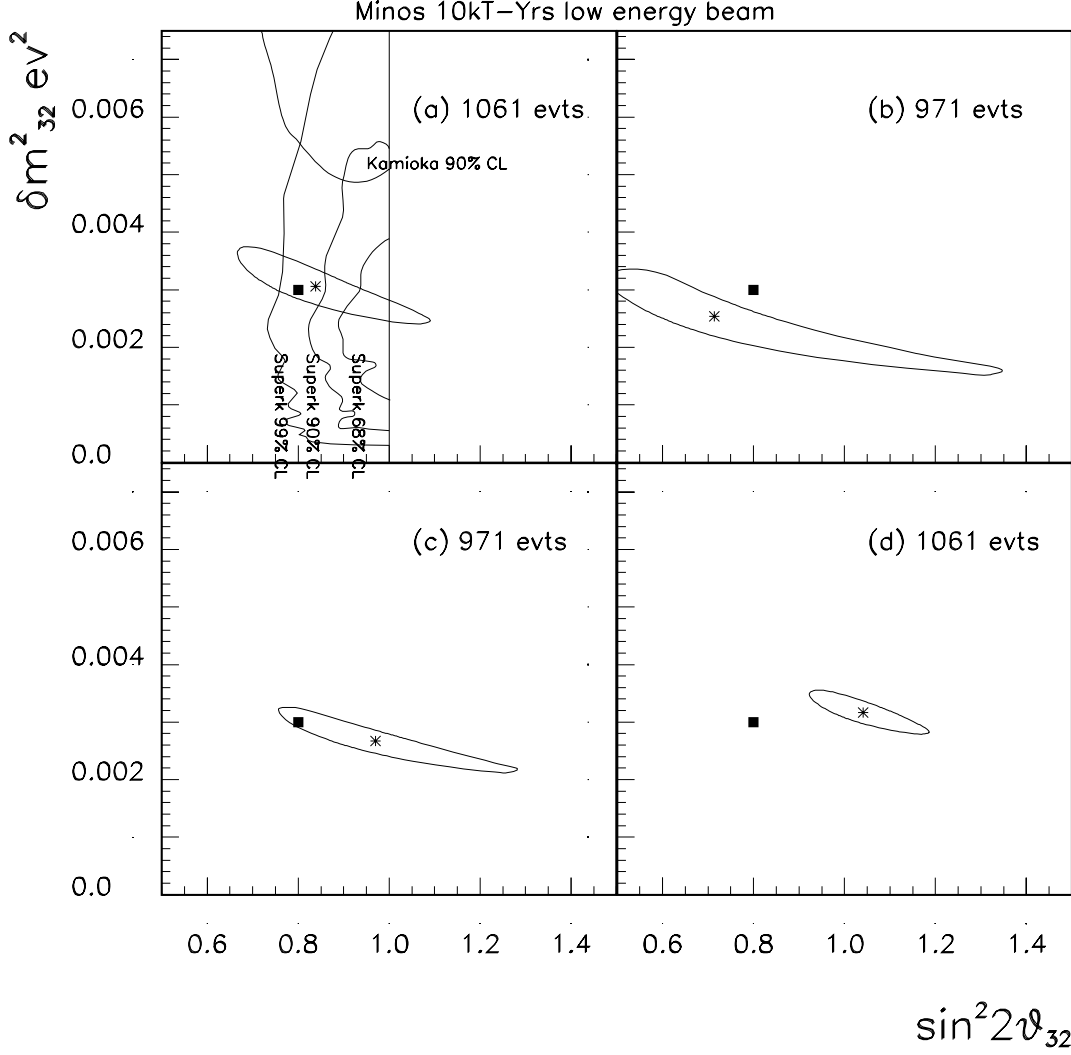


Figure 6: MINOS low energy beam run results for a 10 kiloton-year run. Dark rectangle denotes the generated point of $\sin^2 2\theta_{23} = 0.8$ and $\delta m_{32}^2 = 0.003 \text{ eV}^2$. The \star denotes the fitted point. 90% CL MINOS contour is shown for the cases (a) Geant Fluka spectra used for theoretical curves and experimental results, with SuperK and Kamioka results shown for comparison, (b) Geant Fluka spectra used for theoretical curves and modified spectra used for experimental results, (c) modified spectra used for theoretical curves and experimental results and (d) modified spectra used for theoretical curves and Geant Fluka spectra used for experimental results.

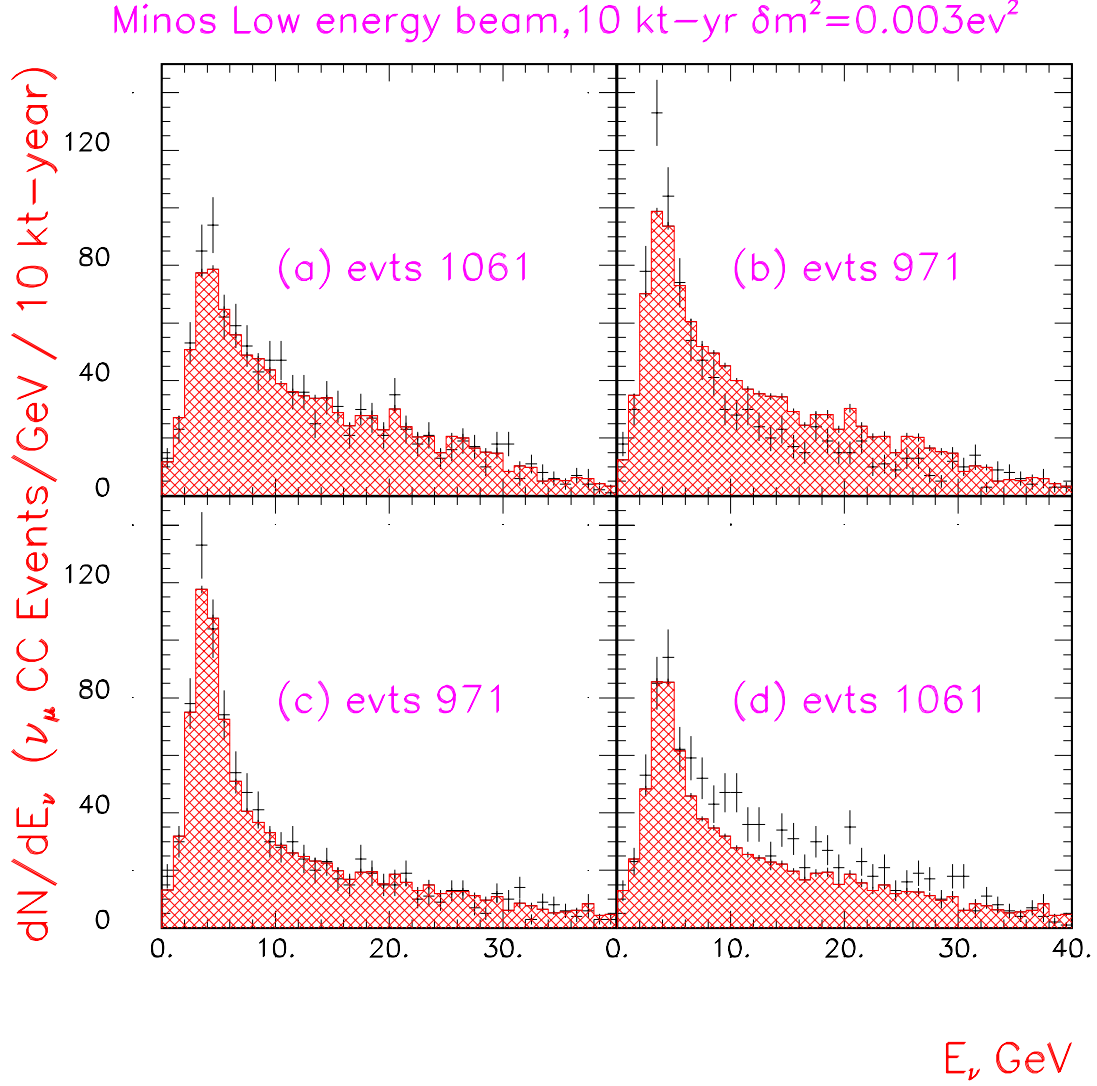


Figure 7: MINOS low energy beam run results for a 10 kiloton-year run. Events generated for $\sin^2 2\theta_{23} = 0.8$ and $\delta m_{32}^2 = 0.003 \text{ eV}^2$. Experimental spectra (histograms with error bars) and fitted functions (hatched histograms) for (a) Geant Fluka spectra used for theoretical curves and experimental results, (b) Geant Fluka spectra used for theoretical curves and modified spectra used for experimental results, (c) modified spectra used for theoretical curves and experimental results and (d) modified spectra used for theoretical curves and Geant Fluka spectra used for experimental results.

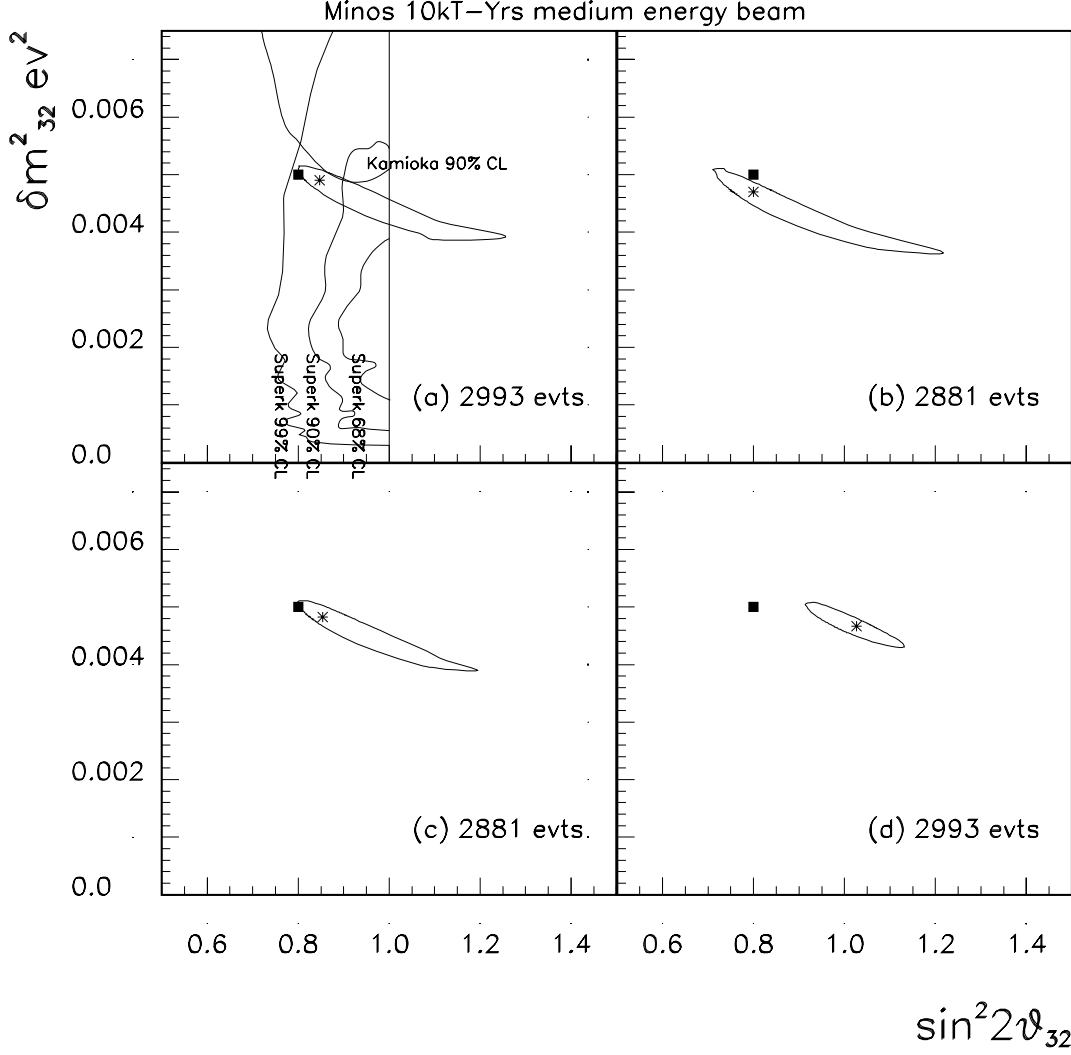


Figure 8: MINOS medium energy beam run results for a 10 kiloton-year run. Dark rectangle denotes the generated point of $\sin^2 2\theta_{23} = 0.8$ and $\delta m_{32}^2 = 0.005 \text{ eV}^2$. The \star denotes the fitted point. 90% CL MINOS contour is shown for the cases (a) Geant Fluka spectra used for theoretical curves and experimental results, with SuperK and Kamioka results shown for comparison, (b) Geant Fluka spectra used for theoretical curves and modified spectra used for experimental results, (c) modified spectra used for theoretical curves and experimental results and (d) modified spectra used for theoretical curves and Geant Fluka spectra used for experimental results.

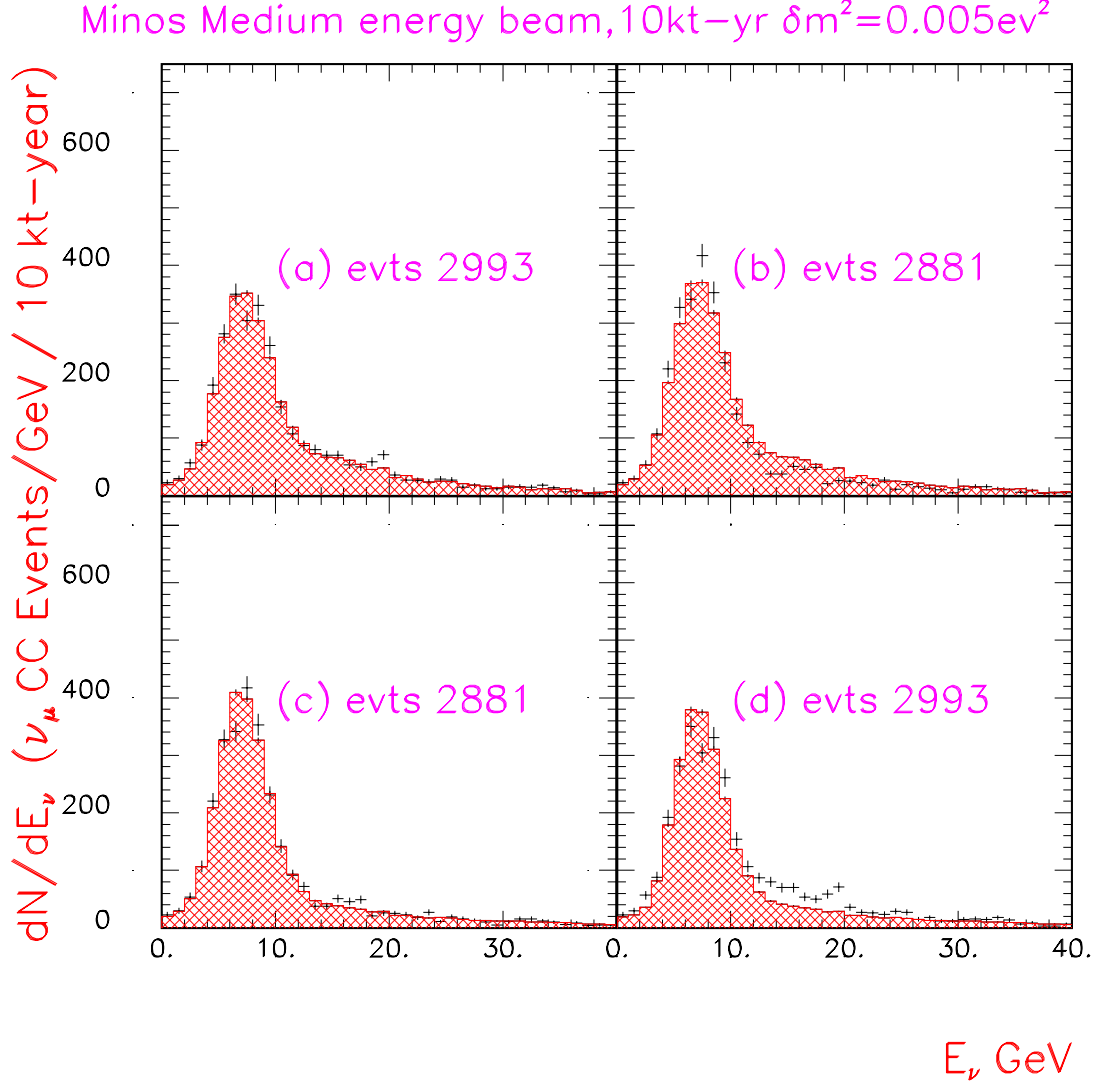


Figure 9: MINOS medium energy beam run results for a 10 kiloton-year run. Events generated for $\sin^2 2\theta_{23} = 0.8$ and $\delta m_{32}^2 = 0.005 \text{ eV}^2$. Experimental spectra (histograms with error bars) and fitted functions (hatched histograms) for (a) Geant Fluka spectra used for theoretical curves and experimental results, (b) Geant Fluka spectra used for theoretical curves and modified spectra used for experimental results, (c) modified spectra used for theoretical curves and experimental results and (d) modified spectra used for theoretical curves and Geant Fluka spectra used for experimental results.

spectra are known in advance. This statement is also true with the proposed “hadronic hose” in MINOS. The performance of the hadronic hose and the near and far detectors can be understood better and with less analysis effort, once the primary particle fluxes and their identity are known to the requisite precision. P-907 provides a method for obtaining these spectra in a timely fashion.

3.4 Proton-Nucleus Physics

High-energy interactions of hadrons in nuclear matter have challenged experiments and theorists for more than fifty years. Initial insights into the physics of hadron-nucleus collisions from cosmic ray emulsions were confirmed by a series of FNAL experiments conducted twenty-five years ago [28, 36]. The phenomenological description of hadron-nucleus collisions which subsequently emerged has survived until the present, largely intact. This description for proton-nucleus collisions, was summarized succinctly by Busza and Ledoux [30],

An incident proton strikes the target nucleus at some impact parameter. It interacts with a nucleon. The nucleon recoils and slow pions are occasionally produced. The incident proton is perhaps slightly excited but basically remains intact. It propagates through the nucleus, colliding with subsequent nucleons. The process repeats ν times, where ν is the number of collisions you would expect a projectile of constant cross section (the inelastic nucleon-nucleon cross section) to make with the nucleons present in the target at that impact parameter. The hadronic matter emerging from the nucleus evolves over a long distance into a multiparticle final state, which depends on ν .

In the meantime, the recoiling nucleons multiply scatter with other nucleons in the nucleus. The nucleus breaks up into nuclear fragments. The number and energy distribution of nuclear fragments and slow particles (primarily recoiling nucleons), and thus the total energy deposited in the target nucleus, is independent of the energy of the incident proton but does depend on the number of nucleons with which the incident proton interacts.

Although the physics contained in this picture is not currently within a tractable realm of QCD, the implicit assumptions about hadronic interactions in nuclear matter have greatly influenced the interpretation of data from heavy-ion collisions, where it is often difficult to find meaningful benchmarks for comparison in the search for new phenomena. The scaling of experimental signatures with the number of participant nucleons are nearly all based upon this physical picture in pA collisions. For example, the excess production of strange baryons in Pb+Pb collisions in CERN NA49 given as evidence for the creation of a new state of matter is relative to the linear extrapolation in number of participant nucleons from lighter systems. In addition, many of the cascade models to which data are compared also assume such a picture. A modification to this picture could have significant implications for the interpretation of existing data in heavy-ion collisions as well as the data that will soon be taken by experiments at RHIC.

This semi-classical picture of pA collisions is arguably simplistic and naive, but the data from pA experiments in the intervening years have not led to a need to revise it. This

is partly because many of the experiments which sought to improve on the initial FNAL counter experiments by identifying final state particles achieved this at very low rates, or in limited regions of phase space. This situation is now being partially addressed by three pA experiments: CERN NA49, and BNL E910 and E941. These experiments combine high data rates with large (though still incomplete) acceptance for identified particles. Furthermore, E910, and to a lesser extent NA49 are able to measure particle production for high values of ν , as determined from the number of recoil protons (see [32] and references therein). Leading particle momenta are measured by a forward calorimeter in E941, and by downstream tracking (proton and Λ only) in E910. As expected, the ability to measure the mean number of projectile-nucleon scatterings and the leading particle momentum are the crucial elements which are now leading us to revise old ideas in hadron-nucleus collisions.

The data from these experiments were presented together recently at the “Workshop on Proton-Nucleus Collisions,” held Feb. 5, 2000 at LBNL. The workshop was held to revisit old theories of particle production in nuclear matter in light of new data, and to examine upcoming opportunities for pA experiments at FNAL and RHIC. It was readily apparent that P-907 is in a position to make unique contributions to further our understanding of this complex topic. In what follows, we present a selection of two topics from the workshop, strange particle production and projectile energy loss, drawing on experimental data (mostly E910) that have been presented publicly elsewhere. This is then followed with some brief remarks on the utility of a broad survey of hadron-nucleus data to the general high-energy physics community.

Enhanced production of strange particles is one of the predicted signatures for observing the phase transition to a quark-gluon plasma in heavy-ion collisions [27]. Experiments at both the AGS and the SPS have observed roughly a threefold increased production of Λ ’s and K ’s per participant relative to the production in pp and inclusive pA collisions. Examples from AGS experiment 866 and SPS experiment WA97 are shown in Fig. 10. Even larger enhancements of 20x per participant have been observed for Ξ^- and Ω^- production and anti-strange baryon production at the SPS. The enhancements at the SPS — consistent with quark-based thermodynamic model predictions for the ratios and in contradiction with various hadronic cascade model results — are cited as evidence for a new state of matter created at the SPS. The strangeness enhancement signature is one of two key pieces of evidence cited in the recent CERN press release [37].

Until now, the situation regarding strangeness enhancement was unclear. Data from E802 at the AGS [23] showed a clear increase in the inclusive K^+/π ratio while measurements at CERN suggested no overall strangeness enhancement [26]. However, measurements of the ν dependence of Λ production in 17.5 GeV/ c pAu collisions recently submitted by E910 [33] indicate a clear increase in the Λ yield per participant with increasing number of scatters of the projectile proton in the Au target. The summary results from this publication are shown in Fig. 11 with the solid line indicating the expected yield if the Λ yield per participant nucleon is the same as in pp collisions at the same energy. For the first 4-5 collisions, the measured Λ yield increases faster than expected from the participant scaling of pp data, and then saturates. A preliminary analysis of the leading Λ production *vs.* ν [40] suggests that excess production relative to participant scaling for $\nu \leq 3$ may be coming from fragmentation of the projectile.

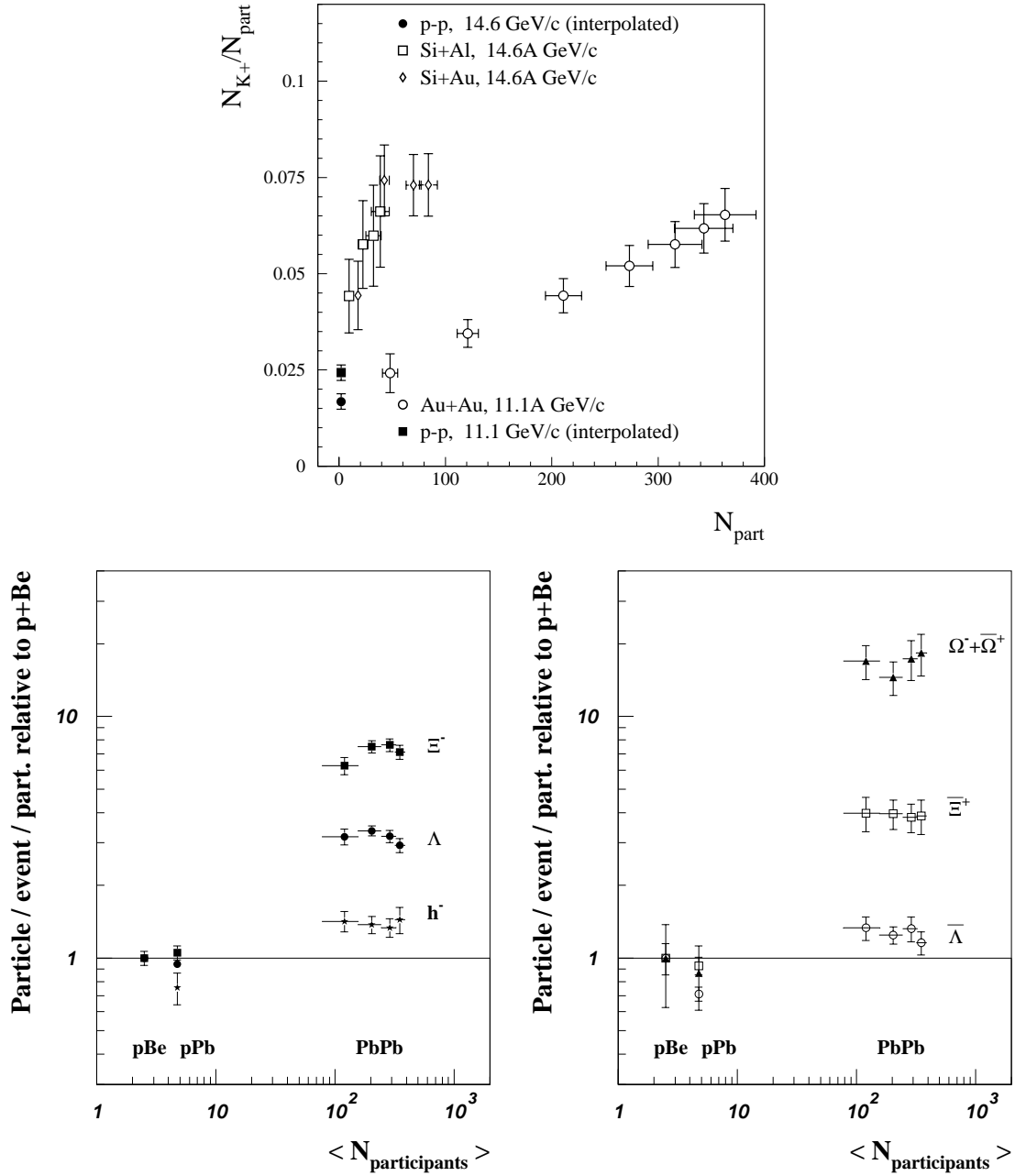


Figure 10: Examples of heavy ion data showing strangeness enhancement. Top - data from AGS E866 showing the K^+ yield per participant *vs.* N_{part} in SiA and AuAu collisions; pp data shown in solid symbols. Bottom - Data from SPS experiment WA97 showing various strange baryon yields per participant relative to pBe collisions.

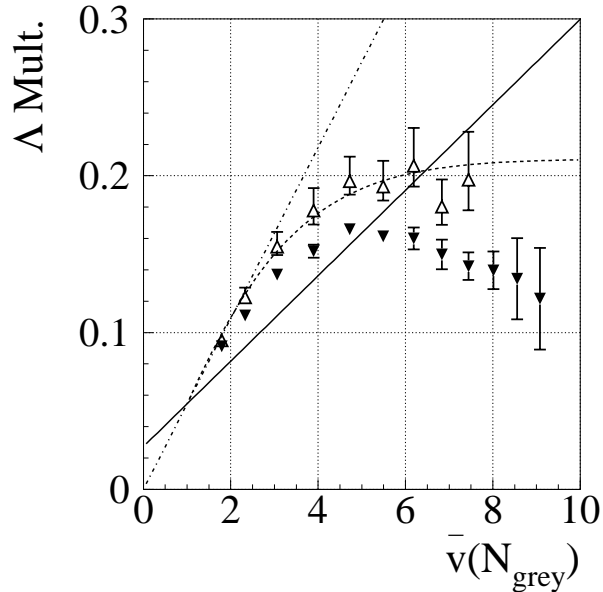


Figure 11: ν dependence of Λ production in 17.5 GeV/c p Au collisions from E910. Solid points show yield within E910 acceptance, open points show estimated total yield. Solid line shows participant scaling of pp data, dot-dashed shows maximal “binary-collision” scaling. Dashed line shows empirical fit, $N_{\Lambda} = N_{pp}(1 - e^{-0.3\nu^{1.3}})/(1 - e^{-0.3})$.

These new results have profound consequences for the interpretation of strange particle production in nucleus-nucleus collisions. If the projectile fragmentation contribution to strangeness is proportional to ν then this mechanism may account for a threefold increase in the Λ and associated K production shown in Fig. 10 for Au-Au and Pb-Pb collisions where $\langle \nu \rangle > 3$. One calculation based on the Constituent Quark Model (CQM) [41] reproduces the observed centrality dependence of Λ and K production in pA accounts for nearly all of the observed enhancement at the AGS and SPS [40, 35].

Though the new centrality dependent measurements on Λ production by E910 may “explain” the observed enhancement for singly strange baryons and associated strange mesons, the greater enhancements observed for Ξ^- and Ω^- production remain an open question. Although E910 analysis for Ξ^- and Ω^- currently in progress may provide some clues, there will not be sufficient statistics to achieve a ν dependence study of the same caliber as was done for the Λ production. With higher beam energies and planned improvements to the TPC data acquisition P-907 can easily make these measurements. If the CQM is an accurate guide, the centrality dependence for multi-strange baryons will be even more pronounced. In the remainder of this section, we use the CQM to estimate the rates and centrality dependence for the production Ξ^- and Ω^- for P-907.

To estimate the centrality of strange baryon production for 120 GeV/c central p Au collisions we attribute 1/3 of the nucleon-nucleon cross-section to calculate the number of wounded quarks, N_{wq} , as in [26], and parameterize the $s\bar{s}$ fragmentation according to Λ production in pp [38] extrapolated to 120 GeV/c [40]. The resultant centrality dependent

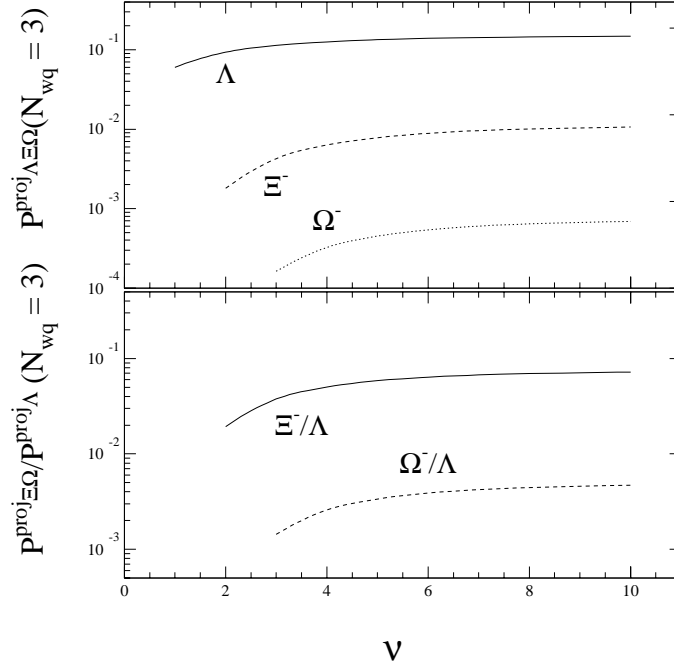


Figure 12: Top - Estimates of Λ , Ξ^- , and Ω^- production from projectile fragmentation in pA collisions as a function of ν based on the constituent quark model (see text for details). Bottom - projectile fragmentation rates for Ξ^- and Ω^- relative to Λ 's.

production rates and ratios of strange baryons are shown in Fig. 12. Note that this model does not allow for multiple quark interactions resulting from single nucleon-nucleon interaction — Ω^- production only occurs for $\nu \geq 3$. The asymptotic production rates in Fig. 12 for $N_{wq}=3$ are given by,

$$N_{\Lambda/\Sigma^0} = 2(1 - \gamma)^2\gamma, \quad (2)$$

$$N_{\Xi^-} = \frac{3}{2}(1 - \gamma)\gamma^2 \quad (3)$$

$$N_{\Omega^-} = \gamma^3, \quad (4)$$

where, from the pp inclusive Λ production estimate for 120 GeV/ c ,

$$\gamma = \frac{3}{4}N_{\Lambda}^{pp} = (9.0 \pm 0.8) \times 10^{-2}. \quad (5)$$

For central collisions of protons with heavy nuclei we therefore expect a projectile fragmentation Ω^- yield of 7.0×10^{-4} per central collision, roughly ten times larger than the production at 18 GeV/ c . An event sample of 2×10^6 centrally triggered events would yield a sample of about 1×10^3 Ω^- produced by projectile fragmentation which decay to ΛK^- . WA97 has measured a rate of 2×10^{-4} for total Ω^- production in pPb collisions with no

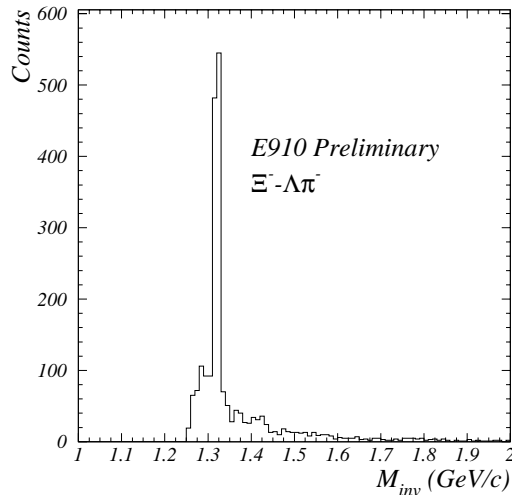


Figure 13: Invariant mass plot for $\Lambda\pi^-$ pairs. See text for details.

centrality selection and for a narrow rapidity range, $|y - y_{\text{cm}}| < 0.5$, where $y_{\text{cm}}=2.91$ [25]. For comparison, the published event sample for WA97 comprises 15 Ω^- and 4 Ω^+ .

Fig. 13 shows a clean invariant mass plot for approximately 900 Ξ^- identified $\Lambda\pi^-$ pairs, with cuts on the distance of closest approach (<5 cm), interaction vertex (0.12 cm from center of target), and decay vertex (>2.5 cm downstream of target).

The CQM provides a framework for understanding the centrality dependence of Λ production in pA that is more useful than the prevailing description of pA collisions set forth earlier. Indeed, this is perhaps the simplest revision imaginable, where the fragmenting nucleon is now replaced with quark-fragmentation in the CQM. Yet the strangeness enhancements observed in pA and the consequences for the enhancement in AA do not themselves depend on the validity of the CQM. The essential point is that if we are to search for new states of matter in high energy, centrally triggered AA collisions, it behooves us to compare those results to pA data for which the effects of the same *centrality* requirement can be measured. E910 has demonstrated that the EOS TPC can measure collision centrality in pA .

One question which has been with the heavy ion community for some time but which has yet to receive a satisfactory answer is the question of projectile energy loss, or stopping. There are two facets of this question which go directly to the heart of where (in phase space) one might expect to find the deconfinement phase transition, and what can be learned from it.

- How much thermal energy is deposited in the central region?
- What is the baryon density in the central region?

These are difficult measurements to make in heavy ion collisions, especially in a collider where the outgoing beams place physical limits on accessible detector space. The answer to the first question above is further complicated in a collider by hard-scattering processes. In what follows we concern ourselves only with measuring the forward energy component,

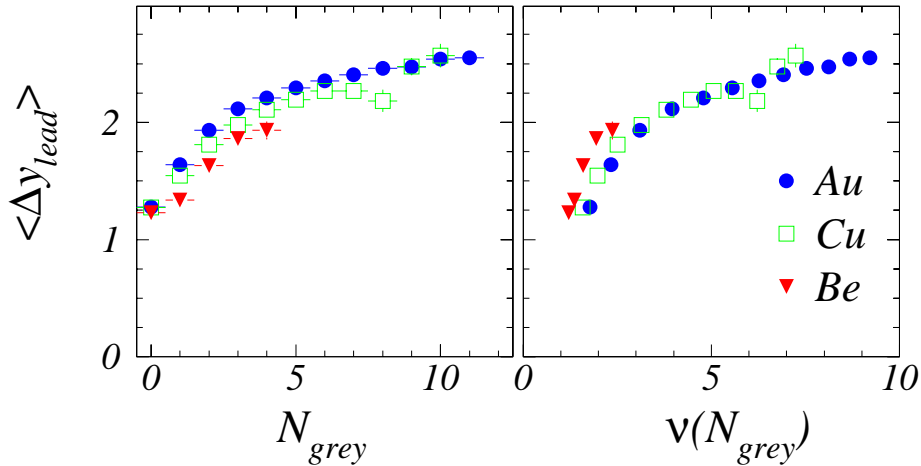


Figure 14: $\langle \Delta y \rangle$ for 18 GeV/ c vs. the number of recoil nucleons measured in the TPC, N_{grey} , and ν extracted from this quantity.

which remains an essential element in understanding the total energy deposition. Again, pA collisions are crucial to understanding the underlying mechanics of energy deposition, and again it is the central pA collisions which will prove most important for testing how well we understand the energy loss mechanisms and for setting limits on the maximum energy deposition attainable in heavy ion collisions.

The first estimate of maximum “nuclear stopping power” was made by Busza and Goldhaber [29] for 50% central pPb collisions. Using simple but clear assumptions about the shape of the leading baryon rapidity loss (Δy) distributions and constraining these shapes with the available data [14], they predicted a value of $\langle \Delta y \rangle = 2.4$ for 50% central. Following this prediction, a set of central 100 GeV/ c pAu events [39] provide a weak consistency check, and a similar data set at 200 GeV/ c [24] yields a mean rapidity loss of 2.4. Thus sparse data and preliminary analysis indicate the initial estimates of [29] may be correct; we still wish to know the maximum energy deposition for the most central pA collisions.

E910 has measured the $\langle \Delta y \rangle$ as a function of ν for the 18 GeV/ c beams and targets of Be, Cu, and Au [31]. The results of this analysis are shown in Fig. 14. The values of $\langle \Delta y \rangle$ fall nearly on top of a single curve for the three targets when plotted vs. ν . The values of $\langle \Delta y \rangle$ rise quickly after a few collisions and then saturate at a rapidity loss of 2. It is not possible to say whether this saturation is due to the kinematic limit for a beam of 18 GeV/ c ($y_{beam} = 3.6$) or whether a fundamental limit has been reached. A higher energy beam is needed. With the TPC to measure recoil protons, downstream tracking of the leading particle momentum, and a beam rapidity of 5.5, P-907 is uniquely capable of providing a definitive answer to the question of energy loss in pA collisions.

Finally, we briefly consider the implications of the CQM for the question of energy loss. In this case, the leading baryon is replaced by leading constituent quarks, which may reside in one, two, or three particles that retain some memory of their forward momentum. The

nature of the analysis changes the measurement of forward particle distributions can still be used answer questions of energy/baryon density in A-A collisions. See [34] for a thorough treatment of this topic.

The situation for strange particle production and forward particle distributions in pA collisions are two of the most striking examples of a general lack of data for hadron-nucleus collisions. A survey of the literature turns up enormous gaps for measurements of inclusive particle production cross-sections and total inelastic cross-sections in the range 1-120 GeV/ c . Data exist for a small subset of targets and beam energies. Furthermore, when overlapping measurements exist they often have large systematic discrepancies. This is often significant for many users of high-energy nuclear physics data.

As part of the pA program, we propose to fill in these gaps with a carefully chosen set of beam momentum and target species. The details of this part of the pA program are given in sections 4.2 and 4.3 on rates and beam requests.

3.5 Measurements for Atmospheric Neutrino Physics

The most compelling of the existing neutrino anomalies is the atmospheric neutrino anomaly. The multiple and mutually corroborative observations by the Superkamiokande experiment are sufficiently strong as to make the oscillation interpretation of these data almost certainly correct [42][43].

The single largest uncertainty in the atmospheric neutrino analysis comes from the uncertainty in the incident neutrino flux ($\Phi(\nu)$)—the flavor composition of the incident neutrinos, and their energy and angle distributions. Cosmic rays hitting the earth’s atmosphere produce pions, which decay into muons, which in turn decay into electrons. This chain, $\pi \rightarrow \mu\nu_\mu \rightarrow e\nu_e\nu_\mu\nu_\mu$, produces twice as many ν_μ as ν_e . There are, however, contributions from K^\pm and K_L^0 to the $\Phi(\nu)$, and these become increasingly important at higher energies. The sources of errors in the atmospheric neutrino flux are shown in in Table 1.

Table 1 shows that the uncertainty in the neutrino flux, in turn, is dominated by the uncertainty in modeling the hadronic interaction of the primary cosmic hadrons with the earth’s atmosphere resulting in the production of parent mesons — π ’s and K ’s. We do not know how to calculate the multiplicities and the momentum distributions of the secondary mesons. The uncertainty in the π and K distributions translates to an error of about 30–40% in the estimation of the neutrino flux. In fact, the difference in prediction of the atmospheric neutrino normalization, $\Phi(\nu_\mu)$ and $\Phi(\nu_e)$, between the Bartol and Fluka packages is as large as 25–30% at around E_ν of 5 GeV. The actual error must be still larger. The flavor-ratio, μ/e , is more robust, and is believed to be at the 7% precision.

The error in the neutrino cross-section, particularly at low energies, is surprisingly large. Nevertheless, measurements in a “Near” detector—such as at K2K or other planned experiments—will entirely eliminate this source of error.

The precision interpretation of the atmospheric neutrino data, leading to an accurate determination of the oscillation parameters, requires a dramatic improvement in our knowledge of the π/K production ratio. The relevant energy range of atmospheric neutrinos is from 0.2 to 100 GeV. This roughly corresponds to the meson energy range from 1 to 400 GeV. The existing data by Atherton *et al.* [44] and the SPY collaboration [45] well cover the high

Table 1: Sources of Error in Prediction $\Phi(\nu)$:

Source of Error	Fractional Contribution to $\Phi(\nu)$
Primary Flux	5–10%
Hadronic Interactions	
$\Phi(\nu)$ (Normalisation)	30–40%
$\Phi(\nu_e)/\Phi(\nu_\mu)$ (Ratio)	7%
Neutrino Cross-Section	20%

energy range (> 100 GeV) of meson production. One of the goals of P-907 is to cover the crucial 5 GeV to 100 GeV range.

P-907 will measure the meson production cross-section by protons *and pions*. The momentum of the proton beam can be varied from ≈ 5 GeV/ c to 120 GeV/ c . Not only will we precisely determine the charged pion and kaon spectra, but also, uniquely, the K_S^0 spectrum which will tell us the K_L^0 contribution to the neutrino flux.

3.6 Neutrino Factory Needs

Current schemes for neutrino factories[46] [47] envisage production and collection of pions using 16 GeV/ c protons[46] and ≈ 2 GeV/ c protons [47]. While these measurements will be made by the HARP experiment at CERN [4], there are other proton drivers being considered for the neutrino factory, namely the Brookhaven AGS (24 GeV/ c protons) and the proposed Japanese Hadron Facility machine (50 GeV/ c protons). P-907 is ideally suited to making these higher energy measurements. As the design of the targets proceed, it would be useful to measure particle production off the actual target design in question rather than rely on Monte Carlos to predict the behavior of the showers. Facilities such as the one proposed here would permit such measurements to be made in the future.

3.7 Quality of Existing Hadroproduction Data

Current hadronic production Monte Carlos such as MARS[6] and GEANT [7] employ extensive schemes that rely on existing data as a function of the kinematic variables of particle production as well as a function of the atomic mass A of the nucleus.

One such a phenomenological model by P-907 collaborators Mokhov and Striganov[8] uses experimental data on pion production for proton beams on various nuclei to parameterize the cross section as a function of x_F , p_\perp and the atomic mass A . The model shows excellent agreement with experiment on pion production at proton momenta $p_0 < 30$ GeV/ c for light, medium and heavy nuclei. While it is beyond the scope of this proposal to review all the existing hadroproduction data, it is instructive to review some of the data acquired over the years to point out the difficulties encountered with the sparseness of the data and with phenomenological models for primary momenta around 100 GeV/ c .

Fig. 15 shows the π^- production cross section as a function of x_F , the Feynman variable, at $p_\perp=0$ for protons of various momenta ranging from 67 to 450 GeV/ c incident on Be nuclei.

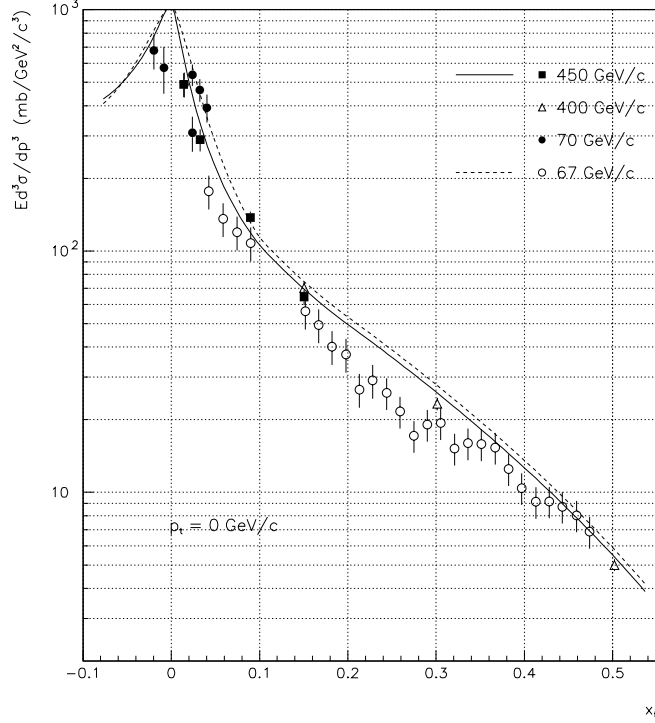


Figure 15: Invariant cross section of π^- production in $p\text{Be}$ interactions as a function of Feynman x for $p_t=0$ GeV/ c . Symbols - experimental data; curves - model calculations.

The 70 GeV/ c data[12] is obtained by extrapolating Al, Cu and W data to Be using a fitted A^α power dependence. The curves represent model calculations for incident momenta of 67 GeV/ c and 450 GeV/ c . The model reproduces the CERN [10], [11] and part of Serpukhov [12] data rather well, but there is a noticeable disagreement around $x_F=0$ between two measurements of the same group [12].

Fig. 16 shows the π^+ production cross section as a function of x_F at $p_\perp=0$ for protons of various momenta ranging from 67 to 450 GeV/ c incident on Be nuclei. The curves represent model calculations for incident momenta of 67 GeV/ c and 450 GeV/ c . As can be seen, the data of the various groups differ from each other drastically. The model agrees with some data but differs considerably from the others. The NA44 point at $x_F=0$ seems anomalously high, and is not reproduced by the other experiments or the model. It seems that data [9] at 67 GeV/ c is too low for the production cross section. To check this point we compare measurements of π^+ production cross section for $p_\perp=0.5$ GeV/ c (Fig. 17). It is seen that CERN [10] (400 GeV/ c) and FNAL [14] (100 GeV/ c) data agree well for $x_F \geq 0.3$ (it is also true for other p_\perp and negative pions). But again the NA44 data at $x_F \sim 0$ differs by 50% from both the model and the other data.

Fig. 18 shows the transverse mass distribution ($m_T = \sqrt{p_T^2 + m_\pi^2}$, m_π is pion mass) of π^+ for several intervals of the lab rapidity y_{lab} for proton momentum of 450 GeV/ c . SPY and NA44 measurements have different transverse momentum dependences at low p_\perp .

These illustrations demonstrate that the data taken by many experiments have systematics in them that are poorly understood. It would be good to have one experiment make measurements over many momenta and incident particle species. The excellent rate, mo-

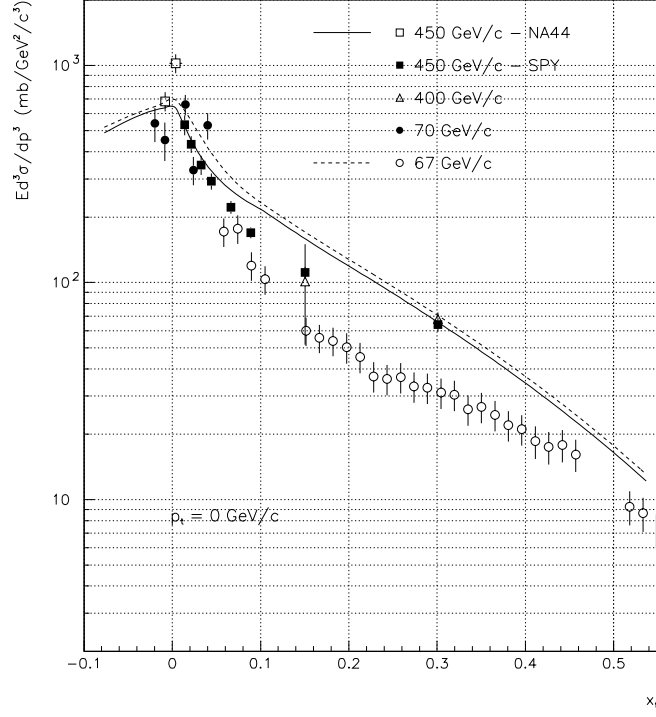


Figure 16: Invariant cross section of π^+ production in $p\text{Be}$ interactions as a function of Feynman x for $p_t=0 \text{ GeV}/c$. Symbols - experimental data; curves - model calculations.

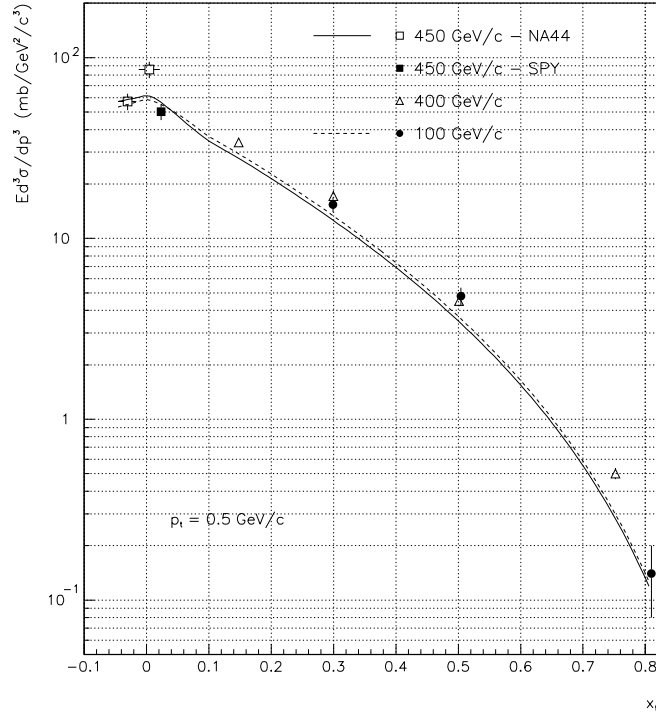


Figure 17: Invariant cross section of π^+ production in $p\text{Be}$ interactions as a function of Feynman x for $p_t=0.5 \text{ GeV}/c$. Symbols - experimental data; curves - model calculations.

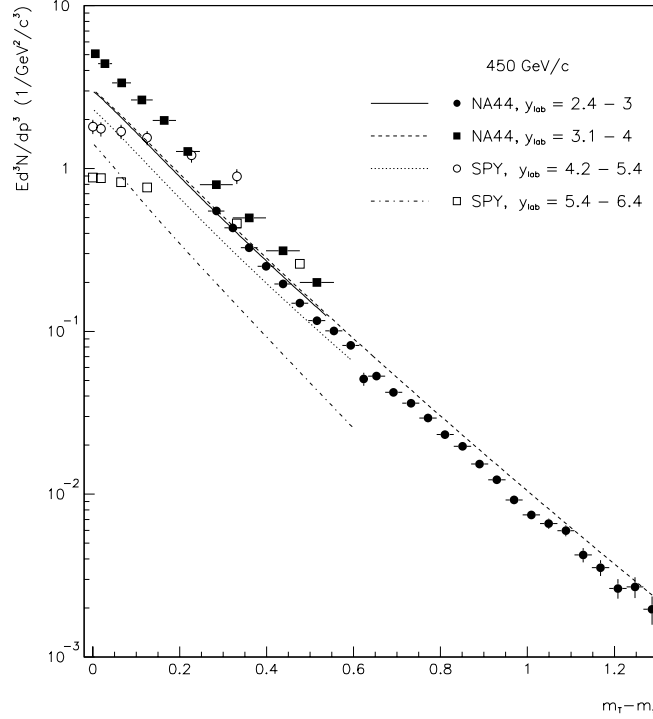


Figure 18: Invariant cross section of π^+ production in $p\text{Be}$ interactions as a function of the transverse mass $m_T = \sqrt{p_T^2 + m_\pi^2}$ of the π^+ . Symbols - experimental data; curves - model calculations.

momentum range and particle identification capabilities of P-907 are unmatched in this regard by competing experiments and can dramatically alter the quality of our understanding of fundamental hadronic processes, if performed in a timely fashion.

3.8 Light Meson Spectroscopy

The spectrum of light ($q\bar{q}$) mesons was described in the early to mid-60's by $\text{SU}(3)$ and $\text{SU}(6)$ symmetries of valence quark combinations. The advent of QCD in the early 70's led to the expectation that additional degrees of freedom (*i.e.* color) could be expressed by a new set of “mesons,” the properties of which would fall outside of $\text{SU}(6)$ multiplets. These states could be formed by gluon aggregates (*e.g.* gg , “glueballs”), quark-gluon hybrids ($q\bar{q}g$), multi-quark assemblies (*e.g.* $q\bar{q}q\bar{q}$, $qqq\bar{q}\bar{q}$, $qqqqqq$ *etc.*) and hadronic molecular states (loosely bound hadron composites). It should be noted that none of these expectations follow rigorously from QCD. In addition, the computational difficulties imposed by QCD in the low energy regime of the light mesons make firm predictions based on calculations difficult. A discussion of some of these issues can be found in [19].

The experimental aspects of light meson spectroscopy involve searching for mesons which do not “fit” into the $\text{SU}(6)$ multiplets. This requires that the meson is observed and a spin and isospin determination is made. Additional information about the meson's identity is provided by its production mechanism and its decay rates to known mesons. There is no conclusive evidence for gluonic states or hybrids from 30 years of experimental work.

Table 2: Meson multiplet assignments form.

$N^{2S+1}L_J$	J^{PC}	$u\bar{d}, u\bar{u}, d\bar{d}$ I=1	$u\bar{d}, u\bar{u}, d\bar{d}$ I=0	$\bar{s}u, \bar{s}d$ I=1/2
1^1S_0	0^{-+}	π	η, η'	K
1^3S_1	1^{--}	ρ	ω, ϕ	$K(892)$
1^1P_1	1^{+-}	$b_1(1395)$	$h_1(1170), h_1(1380)$	K_{1B}
1^3P_0	0^{++}	$a_0(980)/a_0(1450)$	$f_0(400 - 1200)/f_0(980)/f_0(1370)$	$K_0^*(1430)$
1^3P_1	1^{++}	$a_1(1260)$	$f_1(1285), f_1(1510)$	K_{1A}
1^3P_2	2^{++}	$a_2(1320)$	$f_2(1270), f_2'(1525)$	$K_2^*(1430)$
1^1D_2	2^{-+}	$\pi_2(1670)$		$K_2(1770)$
1^3D_1	1^{--}	$\rho(1770)$	$\omega(1600)$	$K^*(1680)$
1^3D_2	2^{--}			$K_2(1820)$
1^3D_3	3^{--}	$\rho_3(1690)$	$\omega_3(1670), \phi_3(1850)$	$K_3^*(1780)$
1^3F_1	4^{++}	$a_4(2040)$	$f_4(2050), f_4(2200)$	$K_4^*(2045)$
2^1S_0	0^{-+}	$\pi(1300)$	$\eta(1295)$	$K(1460)$
2^3S_1	1^{--}	$\rho(1450)$	$\omega(1420), \phi(1680)$	$K^*(1410)$
2^3P_2	2^{++}		$f_2(1810), f_2(2010)$	$K_2^*(1980)$
3^1S_0	0^{-+}	$\pi(1770)$	$\eta(1760)$	$K(1830)$

Table 2 shows the current state of the multiplet assignments, taken from [20]. Many of these assignments are controversial, many have been observed by single experiments, some multiplets have multiple assignments.

The future experimental prospects for light meson spectroscopy are limited. The canonical experiment has a broad, featureless angular acceptance with particle identification throughout the accepted kinematic range. Further, the acceptance of the spectrometer should cover a wide kinematic range to include many production mechanisms (*e.g.* central production via Pomeron-Pomeron interactions, forward production one-pion exchange, *etc.*) thus minimizing systematic effects in the analysis. The experiment should be able to detect γ , π^0 , η as decay products. The ability to study meson production from π , K , p beams simultaneously further strengthens the interpretation of the results by minimizing systematics. Finally, the sample size of the data must be large enough to provide statistically significant results. Planned experiments are: the Large Acceptance Spectrometer (CLAS) ($e - Nucleon$) at TJNAF, COMPASS at CERN, as well as a number of existing experiments which may find additional running time.

P-907 could also be used for a “first phase” light meson spectroscopy experiment, the lack of γ detection being its major deficiency. With event rates of order 10^6 to 10^7 events per day, relatively large samples of events can be recorded for later analysis. The kinematic reach of the detector is very large, extending to large $|x_F|$ (a proton sitting at rest in the rest frame of a 120 GeV/c pp interaction would have roughly 8 GeV/c momentum in the lab frame, a well measured momentum regime in this experiment). For “glueball” searches, the central production region ($|x_F| = 0$) is of particular interest. The double-diffraction

cross sections are traditionally estimated to be $\sigma_{DD} = (4/3)\sigma_D^2/\sigma_{el}$ per target nucleon in pp interactions [21]. This is of order 1 mb in this energy regime. The expected rate of light meson production is then $(1 \text{ mb}/40 \text{ mb}) \times 10^6 \text{ events/day} = 2.5 \times 10^4/\text{day/nucleon}$ for $pN \rightarrow pXN$ events (where N is a proton or a neutron). A 10^6 to 10^7 event sample could be gathered in a 100 day run. The run should be at the largest beam momentum possible to ensure the largest M_X . This sample size is small compared to other samples currently being analyzed [22] but large compared to other surveys (*e.g.* WA76, WA91, *etc.*) in specific kinematic regions.

A second phase experiment with γ detection for π^0 and η detection ability and target region detector would vastly improve the physics reach of this detector. Very long run periods might be possible with the Main Injector schedule in the next few years allowing large data sets to be collected and analyzed. Finally, a first phase run would allow us to look at the possibility of triggers which might greatly enhance the collection of non- $q\bar{q}$ meson events. There exist several calorimeters at Fermilab capable of providing the requisite γ detection.

4 Beam and Experimental Layout

4.1 Implementation Scheme

The experiment consists of two magnetic spectrometers placed in series to cover the complete range of particle production from target to projectile fragmentation regimes with unambiguous particle identification and excellent momentum resolution. The target, which can vary from liquid hydrogen to various nuclei or the long NUMI target, sits upstream of a time projection chamber which sits in a magnetic field supplied by the dipole magnet 1. The TPC can identify charged particles in the low energy regime by dE/dx and some resonances through their decay topology. Immediately downstream, a series of drift chambers, a Čerenkov counter and a Time of Flight (TOF) wall provide tracking and identification for the medium energy regime (1–17 GeV/ c). The second spectrometer has a significantly stronger dipole magnet, a series of drift chambers, and a RICH detector, for tracking and particle identification up to the beam energies.

To reduce cost and accelerate installation, we plan to use existing detectors where possible. Our present simulation incorporates the geometry and field of the Jolly Green Giant magnet originally of E690, and the TPL-B magnet. The Jolly Green Giant has inner dimensions of 230 x 170 x 225 cm. We assume a dipole field of 4 kG, yielding a p_T kick of just 0.35 GeV/ c in the configuration shown. The TPC has been acquired by Fermilab and moved from Brookhaven. The TPC has dimensions of 96 x 75 x 150 cm, and consists of 128 consecutive pad-rows, each with 120 pads per row. In addition to 3D space point tracking, it provides particle identification through dE/dx . It has been quite successfully used by the E910 collaboration in the study of 18 GeV/ c proton-nucleus collisions in a similar configuration. The drift chambers are modeled after the larger of the E690 drift chambers, with dimensions 180 x 120 cm, and a resolution of 200 μm . The first spectrometer also makes use of a Čerenkov counter, here taken to be the E690 counter, originally from E766, and recently a part of E910. Its 200 x 125 cm dimensions match the drift chambers, and it has a front mount for one chamber. The light is collected by 96 phototubes after reflection by a set of small mirrors near the center and larger ones towards the perimeter. The inner dimensions of TPL-B are 83 x 32 x 208 cm. It can run with a field of 10 kG for a p_T kick of approximately 1 GeV/ c . For now we show the E690 drift chambers, although slightly larger chambers would be preferable. Particle identification in the downstream spectrometer will come from a RICH detector, here taken to be the SELEX RICH, with a length of 10 m, and a diameter of 2.4 m. The chamber has been used with Neon at 1.05 atm.

We are also investigating the need for a recoil detector (not shown) around the target to identify recoiling particles, such as slow protons and pions. These particles are of particular interest to the p-A and production physics aspects of this proposal. We are pursuing studies to determine if existing detector systems (*e.g.* the old CDF silicon detectors) would be applicable to E907. The purpose of this recoil detector would be to extend beyond the demonstrated TPC wide angle particle acceptance.

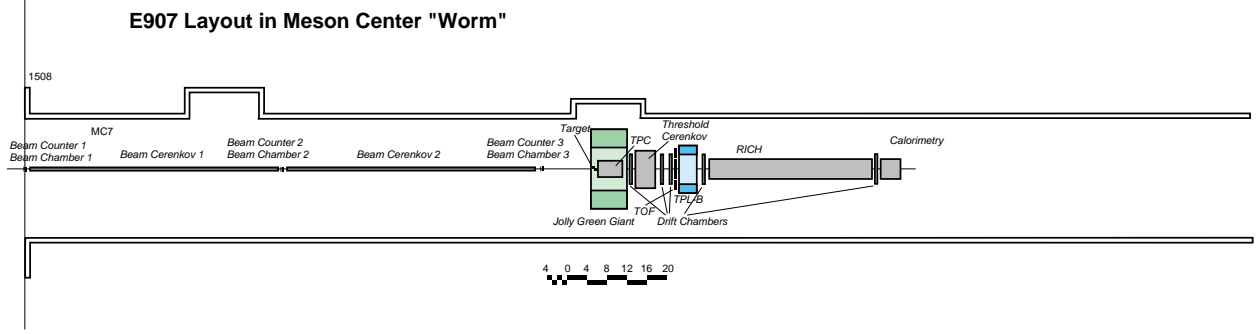


Figure 19: Layout of proposed Meson Center beam line in enclosure MC7.

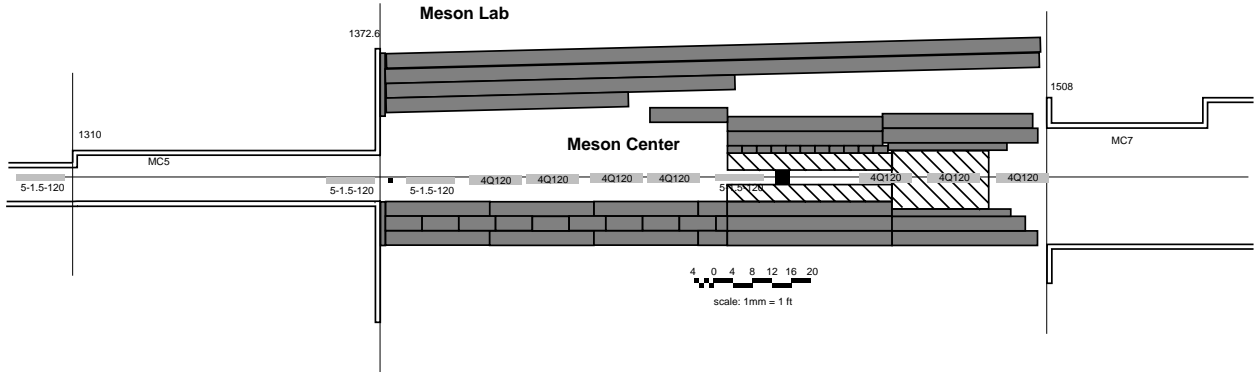


Figure 20: Layout of secondary beamline proposed for Meson Center.

4.2 Beam Requirements

The primary Main Injector beam of 120 GeV/ c is transported into the Meson-Center beam-line, Fig.20. The first two dipole magnets are used to offset the beam 19 cm in the target region so that the beam is back on the normal Meson Center line following the dispersion bends after the target. The target is 2" of Cu, which is 50% of an interaction length. This target is followed by a dipole, creating momentum dispersion at the jaw collimator. A quadrupole doublet (four quadrupoles total) focusses the secondary beam on the collimator, which can be set to select a particular momentum "bite". The dipole just upstream of the jaw collimator puts the beam back on the Meson Center line, albeit reducing the dispersion somewhat. It is there to minimize the beamline length.

Downstream of the jaw collimator are three additional quadrupoles forming an asymmetric triplet. The quadrupoles provide a nearly-parallel beam after the focal point (in fact, they focus the secondary beam on the somewhat distant experimental target). A schematic of the beamline is shown in Fig. 21. Fig. 26 shows the beam envelope at various locations, with the magnet apertures superimposed.

When the beamline is run for the NuMI part of the experiment, the target is removed, the jaw collimator is opened, and one of the quadrupole doublets is turned off.

Radiation losses may limit the beam intensities in the Meson Center beamline to a few 10^{11} protons per spill. A 2" thick Cu target is 50% of an interaction length. The secondary particle yields are shown in Figure 22 for positive particle production and in Figure 23 for

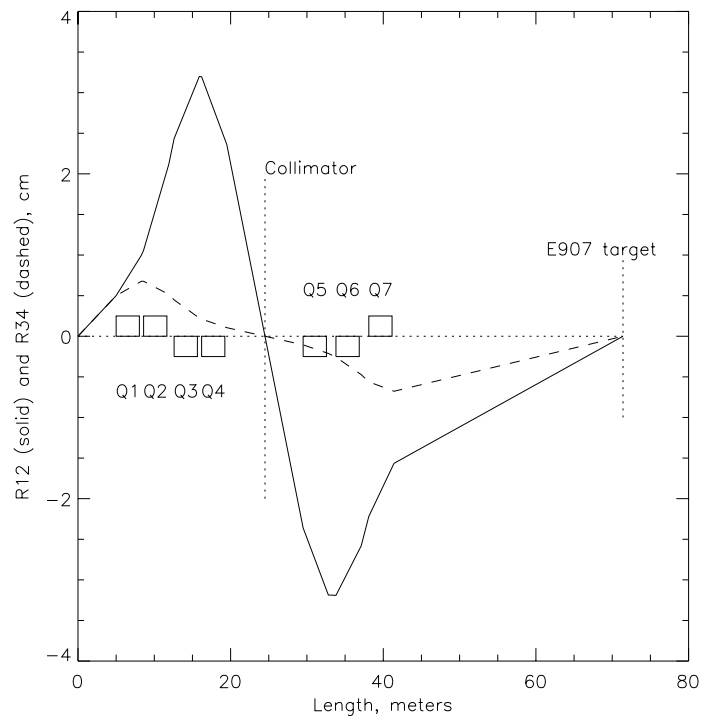


Figure 21: Schematic of secondary beamline proposed for Meson Center with TRANSPORT calculation superimposed.

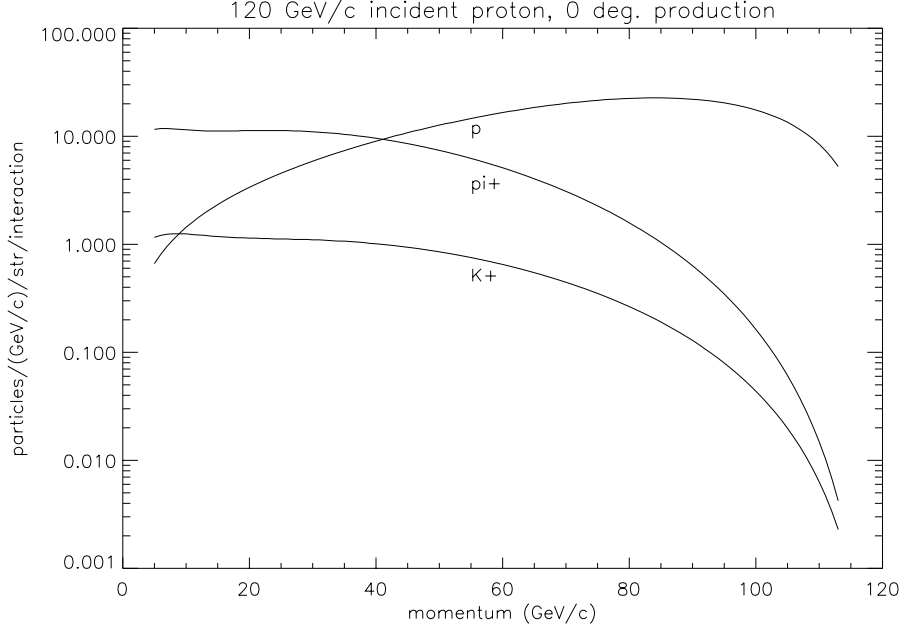


Figure 22: Positive particle production for a 120 GeV/c incident proton beam.

negative particle production. These yields are taken from [51]. The dead time of the TPC is 16 μ s.

Secondary beam instrumentation will include scintillation counters, wire chambers and gas threshold Čerenkov counters. The wire chambers are borrowed from E690 and have an active area of 4" by 6". The details of these chambers are given in [53]. These chambers will be used to measure the incoming beam position and angle.

The Čerenkov counters are used to tag the three primary beam species (π, K, p). This is accomplished by setting the two counters so that: (1) π 's radiate in counter 1, K 's and p 's do not and (2) π 's and K 's radiate in counter 2, p 's do not. The value of the index of refraction of a gas at Čerenkov radiation threshold is shown in Figures 24 and 25. These ranges of indices of refraction are covered by the gases He ($n=1.0000349$), Ne (1.0000671), N_2 (1.000298) and CO_2 (1.000410). Additional Čerenkov counters may be required to eliminate e^\pm background. Special runs will determine the μ^\pm content of the secondary beam.

The length of the counters is determined by requiring the detection of at least 10 photoelectrons. Assuming a collection efficiency of 50% and a detection efficiency of 30% the length of the counter must be 16 m.

4.3 Event Rates

In what follows we will take the Main Injector duty cycle 1 s flat-top every 3 s. We assume that we will receive a spill every cycle. We will also assume that a year is 10^7 seconds long.

Assuming that the total solid angle accepted by the beamline from the 2" Cu target is roughly 10^{-4} (see Fig. 26) the incident beam flux will be roughly $10^4/(10^{-4} \times 0.5 \times 10) = 2 \times 10^7$ protons/spill.

The TPC sets the data acquisition rate. We will assume a trigger rate of 60 Hz. The ion

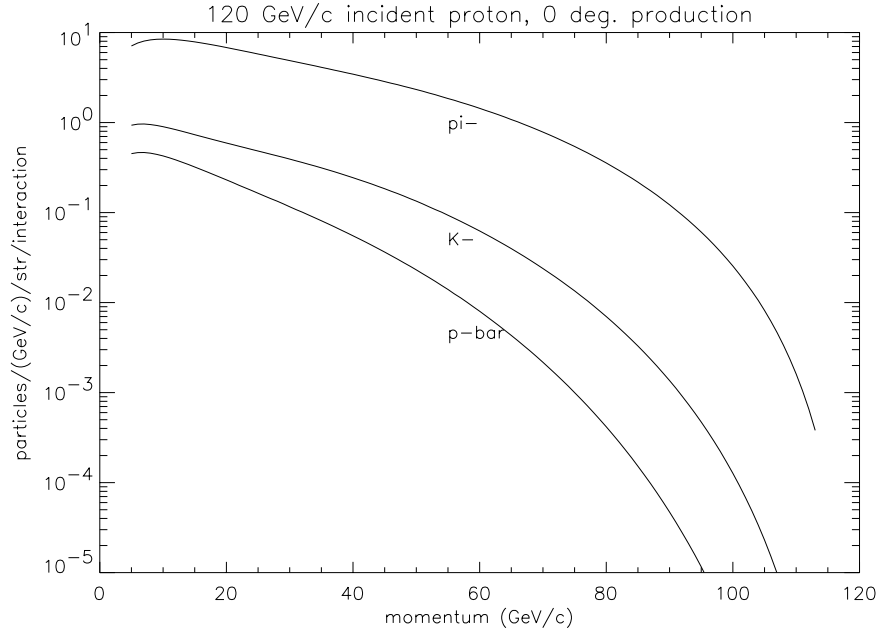


Figure 23: Negative particle production for a 120 GeV/c incident proton beam.

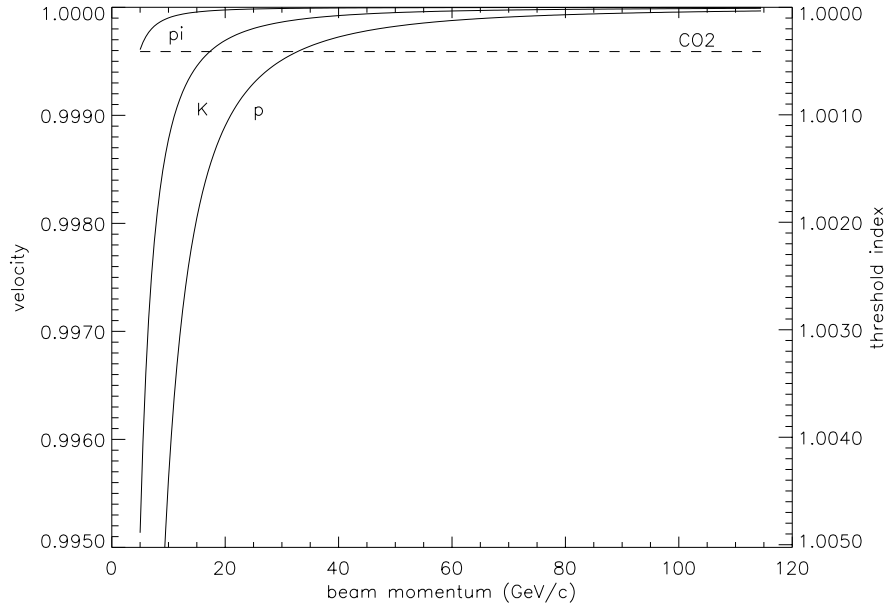


Figure 24: Particle velocities and threshold indices of refraction as a function of secondary beam momentum.

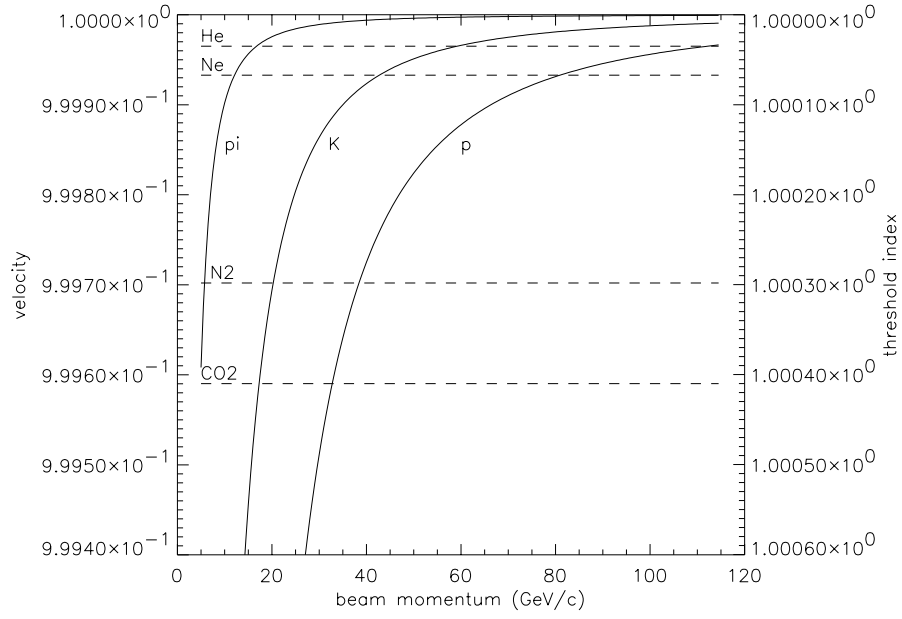


Figure 25: Particle velocities and threshold indices of refraction as a function of secondary beam momentum.

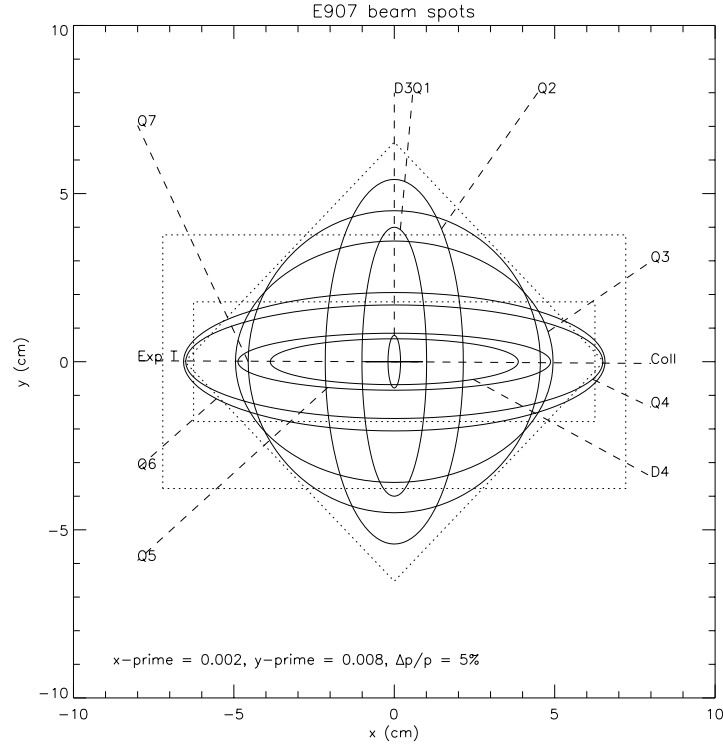


Figure 26: Beam ellipses at 115 GeV/c secondary momentum with magnet apertures superimposed (dotted lines).

Table 3: Particle rates, prescale factors and event yields for a positive secondary beam.

p GeV/ c	p Hz	K^+ Hz	π^+ Hz	p prescale factor	K^+ prescale factor	π^+ prescale factor	p events	K^+ events	π^+ events
5	52.28	58.58	631.37	0.38	0.34	0.03	1000000	1000000	1000000
10	226.54	108.44	1105.01	0.09	0.18	0.02	1000000	1000000	1000000
20	1062.36	165.98	1878.38	0.02	0.12	0.01	1000000	1000000	1000000
30	2783.73	212.66	2507.73	0.01	0.09	0.01	1000000	1000000	1000000
40	5686.32	236.62	2698.51	0.00	0.08	0.01	1000000	1000000	1000000
50	9994.11	229.28	2453.26	0.00	0.09	0.01	1000000	1000000	1000000
60	15691.44	195.47	1925.14	0.00	0.10	0.01	1000000	1000000	1000000
70	22257.07	146.18	1297.94	0.00	0.14	0.02	1000000	1000000	1000000
80	28311.92	93.58	728.22	0.00	0.21	0.03	1000000	1000000	1000000
90	31299.95	48.26	314.94	0.00	0.41	0.06	1000000	1000000	1000000
100	27631.13	17.26	87.21	0.00	1.16	0.23	1000000	862861	1000000
110	14636.48	2.61	8.43	0.00	7.65	2.37	1000000	130727	421312

drift time from the top of the TPC to the bottom is 16 μ s. An uninteracted beam particle will take roughly half this time, 8 μ s, to clear the TPC. Requiring that no “spectator” beam particles be present (on average) will limit the beam rate to 1.25×10^5 Hz. Further, we assume that we use targets that permit 1% of the protons to interact (the relative interaction rates for each beam species is taken to be: $\pi^-:\pi^+:K^-:K^+:\bar{p}:p:0.78:0.58:0.50:0.43:1.13:1.00$).

We use the beam spectra of Malensek [51] to calculate particle fluxes at the detector target. This includes making the target length, primary proton energy and target material corrections to those spectra.

At a 60 Hz interaction rate it is possible to acquire 10^6 events in 42 hours (= 4.63 hrs [beam on] \times 3 [MI duty cycle] \times 3 [overall efficiency]). In practice, we will acquire events from all three beam species (π , K , p) of a given sign simultaneously, prescaling each event rate to saturate the data taking, so that at the end of 126 hours (= 41.7 hrs [per species] \times 3 [species]), 10^6 events are acquired for each charge sign of each species, if possible. Table 3 shows the event rates for p , K^+ and π^+ induced events on target as a function of beam momentum. With a primary beam flux of 2×10^9 protons and a beamline acceptance of 3.2×10^{-6} p (GeV/ c), it shows the beam rates on target for each species, the prescale factors and the total number of events acquired at the end of a 126 hour period. Table 4 shows the event rates for \bar{p} , K^- and π^- induced events on target as a function of beam momentum under the same conditions as for the positive beam.

4.4 Primary Beam Rate Requirements

Using the numbers from Table 3 and Table 4, it is possible to recalculate the beam rate for positive and negative beam running. The maximum beam rate is set by the minimum of:

Table 4: Particle rates, prescale factors and event yields for a negative secondary beam.

p GeV/c	\bar{p} Hz	K^- Hz	π^- Hz	\bar{p} prescale factor	K^- prescale factor	π^- prescale factor	\bar{p} events	K^- events	π^- events
5	37.41	41.42	407.83	0.53	0.48	0.05	1000000	1000000	1000000
10	70.42	69.36	852.41	0.28	0.29	0.02	1000000	1000000	1000000
20	76.32	77.66	1180.99	0.26	0.26	0.02	1000000	1000000	1000000
30	57.68	69.32	1146.29	0.35	0.29	0.02	1000000	1000000	1000000
40	36.55	52.79	997.96	0.55	0.38	0.02	1000000	1000000	1000000
50	19.09	33.64	789.31	1.05	0.59	0.03	954290	1000000	1000000
60	7.95	17.72	554.05	2.52	1.13	0.04	397365	885985	1000000
70	2.51	7.49	334.65	7.96	2.67	0.06	125665	374417	1000000
80	0.55	2.38	165.75	36.26	8.41	0.12	27575	118952	1000000
90	0.07	0.50	61.34	285.46	40.35	0.33	3503	24786	1000000
100	0.00	0.05	13.68	5902.56	406.28	1.46	169	2461	684028

1) rate to set the maximum prescale to 1., 2) rate to set the maximum secondary particle flux to 1.25×10^5 Hz or 3) 3.0×10^{11} protons per spill, the assumed limit for Meson Center. The primary beam rates, secondary beam rates per species and number of events collected in 126 hours are shown in Table 5 and Table 6.

For the NuMI target studies we assume that we will run both the Be and C targets proposed (see [54]). These targets have roughly 70% transmissivity. We have estimated that 10^7 events per target are required to meet the NuMI requirements for predicting the neutrino spectrum at the far detector. The maximum beam rates are set by the requirement that any previous interaction is clear of the TPC volume. The 16 μ s drift time thus limits the primary beam rate to 6.25×10^4 Hz.

4.5 Running Time Requirements

A 3000 hour year allows for 24 “data points”. The calculation of the time required for the various parts of the experiment are shown in Table 7. Note that the H₂ target running is with a 2% target and higher beam flux at high momentum. Our calculated run time is 3400 hours.

Table 5: Primary beam rates, secondary beam rates and event yields for a positive secondary beam.

p GeV/ c	primary protons per spill	p Hz	K^+ Hz	π^+ Hz	total Hz	p events	K^+ events	π^+ events	total events
5	7.65×10^8	2000	5211	41642	48853	1000000	1000000	1000000	3000000
10	3.69×10^8	4178	4651	35138	43967	1000000	1000000	1000000	3000000
20	2.41×10^8	12801	4651	39024	56476	1000000	1000000	1000000	3000000
30	1.88×10^8	26180	4651	40663	71495	1000000	1000000	1000000	3000000
40	1.69×10^8	48062	4651	39325	92038	1000000	1000000	1000000	3000000
50	1.69×10^8	84655	4517	35828	125000	1000000	971069	1000000	2971069
60	1.28×10^8	100766	2919	21315	125000	1000000	627637	1000000	2627637
70	1.01×10^8	112025	1711	11264	125000	1000000	367873	1000000	2367873
80	8.39×10^7	118817	913	5269	125000	1000000	196370	1000000	2196370
90	7.82×10^7	122437	439	2124	125000	1000000	94390	615986	1710376
100	8.99×10^7	124144	180	676	125000	1000000	38768	195914	1234682
110	1.71×10^8	124824	52	124	125000	1000000	11149	35931	1047079

Table 6: Primary beam rates, secondary beam rates and event yields for a negative secondary beam.

p GeV/ c	primary protons per spill	\bar{p} Hz	K^- Hz	π^- Hz	total Hz	\bar{p} events	K^- events	π^- events	total events
5	1.07×10^9	2000	5149	37592	44741	1000000	1000000	1000000	3000000
10	5.77×10^8	2031	4651	42376	49057	1000000	1000000	1000000	3000000
20	5.24×10^8	2000	4733	53356	60089	1000000	1000000	1000000	3000000
30	6.94×10^8	2000	5591	68534	76125	1000000	1000000	1000000	3000000
40	1.09×10^9	2000	6717	94139	102856	1000000	1000000	1000000	3000000
50	1.71×10^9	1636	6707	116657	125000	924377	1000000	1000000	2924377
60	2.49×10^9	989	5128	118882	125000	558816	1000000	1000000	2558816
70	4.19×10^9	526	3647	120827	125000	297365	911704	1000000	2209069
80	8.57×10^9	236	2370	122394	125000	133454	592393	1000000	1725847
90	2.34×10^{10}	82	1347	123571	125000	46250	336739	1000000	1382989
100	1.05×10^{11}	18	604	124378	125000	10095	150918	1000000	1161013

Table 7: Running time requirements for various aspects of E907 running.

Target	“Physics”	Beam Energies	Beam Charges	factor (3×10^6 events/data point)	data points
NuMI 1	MINOS	1	1	3.3	3.3
NuMI 2	MINOS	1	1	3.3	3.3
H ₂	scaling	12	2	1.0	24.0/4
N ₂	atm. ν	3	2	1.0	6.0
Be	p-A	1	1	2.0	2.0
Be	survey	5	2	0.1	1.0
C	survey	5	2	0.1	1.0
Cu	p-A	1	1	2.0	2.0
Cu	survey	5	2	0.1	1.0
Pb	p-A	1	1	2.0	2.0
Pb	survey	5	2	0.1	1.0
total					26.6

5 Detector Performance

5.1 Particle Acceptances

Detector acceptances for the configuration of Figure 27 are shown in Figure 28. The four panels correspond to the following requirements: (a) 10 hits in the TPC, (b) a hit in the Čerenkov, (c) a hit in DC 10, the drift chamber just upstream of the RICH and (d) passage through the mid- z -plane of the RICH. The acceptances were calculated for positive particles (protons) using a simple GEANT implementation of the proposed experimental layout. The target placement is 10 cm before the TPC front window.

The TPC has nearly full acceptance for particles above 0.1 GeV/ c and for $\theta < 80^\circ$, while the Čerenkov acceptance begins at 0.5 GeV/ c , well below the pion threshold, and for $\theta < 15^\circ$. The second spectrometer accepts particles with $\theta < 5^\circ$, with particles above 5 GeV/ c striking the drift chamber prior to the RICH, and particles above 10 GeV/ c traversing at least half of the RICH length.

We examine the worst acceptance case of the NUMI target, and simulate the acceptance assuming all particle production occurs on the front face of the target, 1.22 m upstream from the nominal target placement. The results are shown in Figure 29 for the same four requirements. The TPC acceptance is noticeably poorer, accepting particles with $\theta < 5^\circ$ and the CKOV reduced to $\theta < 10^\circ$. The momentum cutoffs are only slightly higher. Efficiencies in the downstream spectrometer are largely unaffected.

5.2 Particle Resolutions

Using 200 μm resolution for the drift chambers and lever arms of 2 m in tracking we arrive at momentum resolutions of $\delta p/p = 0.05\% \times p$ and $\delta p/p = 0.01\% \times p$ (GeV/ c) for the first and second spectrometers respectively. Given that particles above 5 GeV/ c will be measured in the second spectrometer, we expect to achieve momentum resolution below 10 MeV/ c and approaching 1 MeV/ c over the entire range of particle production. Simulations for the TPC in E910 also yield values which are in this range.

5.3 Particle Identification

The TPC can provide 3σ separation with dE/dx up to 0.7 GeV/ c for π/K and 1.1 GeV/ c for K/p , as well as additional but ambiguous information in the relativistic region. Fig. 30 shows clearly separated Bethe-Bloch bands for μ , π , K , p , d , t , and $\text{He}^{3,4}$ in this momentum range, except where the electron band cross. E910 has been able to identify $\approx 50\%$ of those electrons from pair production using kinematic cuts [56]. Electron contamination is significantly reduced for lighter targets. The particles which lie above the proton band at high momentum are the result of pile-up. A Čerenkov counter identified particles in the mid-momentum range. Filled with Freon 114 the thresholds for π , K , and p are 2.5, 7.5, and 17.5 GeV/ c .

The high end particle identification is nearly complete. Above 7.5 GeV/ c many particles will pass through the RICH and are identified. The proton threshold is already well into the acceptance of the RICH. However, between the TPC and Čerenkov identification regions

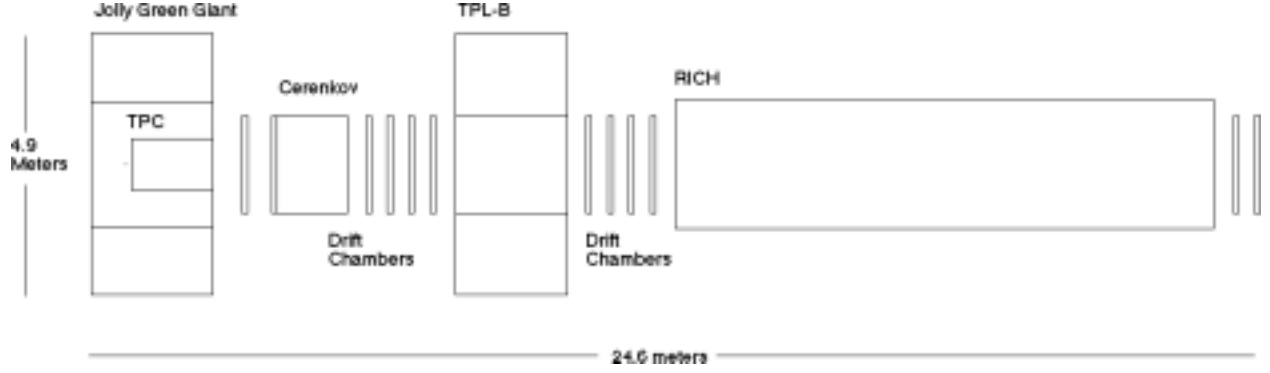


Figure 27: Experiment layout in MC7.

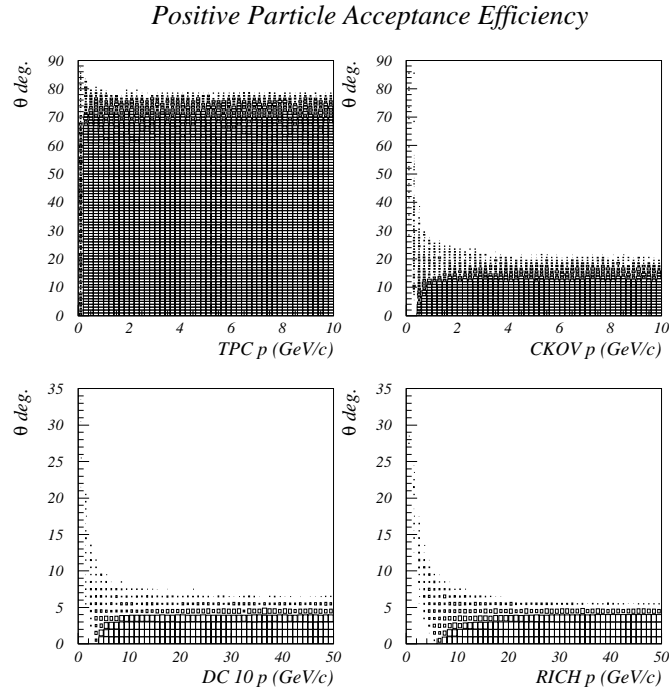


Figure 28: Acceptance efficiencies for 1% interaction targets. Acceptance requirements are (a) 10 hits in the TPC, top left panel, (b) a hit in the Cerenkov, top right panel, (c) a hit in DC 10, the drift chamber just upstream of the RICH, bottom left panel and (d) passage through the mid- z -plane of the RICH, bottom right panel.

NUMI Front Acceptance Efficiency

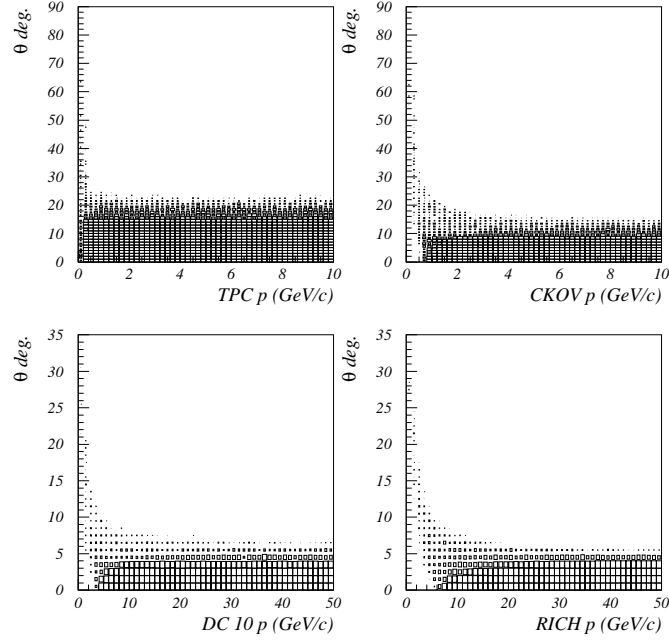


Figure 29: Acceptance efficiencies for the NuMI target. Acceptance requirements are (a) 10 hits in the TPC, top left panel, (b) a hit in the Čerenkov, top right panel, (c) a hit in DC 10, the drift chamber just upstream of the RICH, bottom left panel and (d) passage through the mid- z -plane of the RICH, bottom right panel.

TPC dE/dx Particle ID- BNL E910

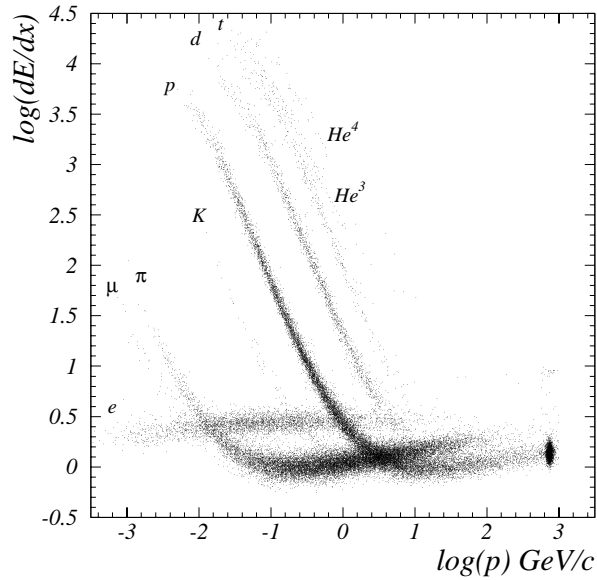


Figure 30: dE/dx particle bands for tracklengths of greater than 50 pads in the TPC. The data are 18 GeV/ c p+Au events from E910.

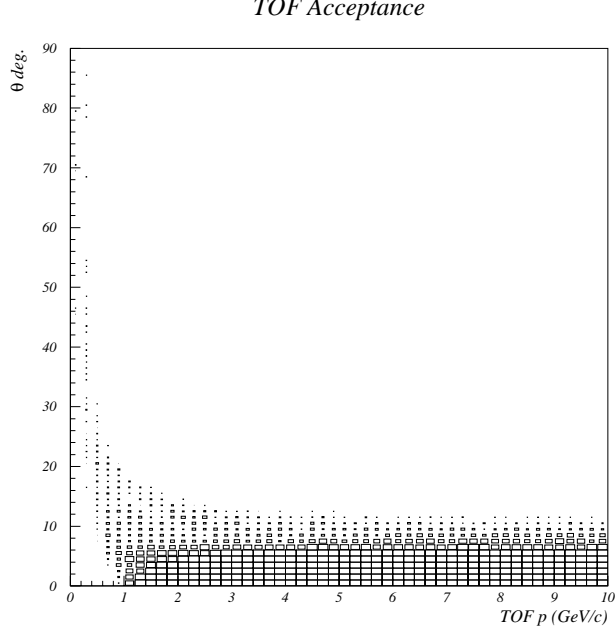


Figure 31: Acceptance efficiency in the TOF for 1% interaction targets.

Table 8: Momentum thresholds (GeV/ c) for three Čerenkov gases.

Gas	π	K	p
Ne	12	42	80
N ₂	6	20	40
CO ₂	5	17	33

there is a significant gap. We have now replaced the final drift chamber before the second magnet with a Time of Flight (TOF) detector, of similar dimensions. The acceptance is shown in Fig. 31. Assuming 100 ps resolutions, we can achieve 3σ particle separation for π/K to 2.7 GeV/ c and K/p to 4.6 GeV/ c .

In the first version of the proposal, incorrect thresholds were given for the Ne-filled SELEX RICH detector. Correct thresholds for three gases under consideration are given in Table 8.

The maximum momentum for particle identification in the RICH is determined by the ring radius resolution. SELEX has achieved a resolution of $\sigma_R = 1.7$ mm, determined primarily by the PMT size and the number of PMT hits [55]. For N₂ and CO₂, the ring radii are roughly two times larger. This gives a 4x higher photon yield, but also leads to questions concerning ring containment. For the present we assume sufficient acceptance to yield $\sigma_R = 2$ mm for the choice of CO₂, leading to 3σ separation of π/K up to 80 GeV/ c , and 134 GeV/ c for K/p .

A second issue is the increased dispersion of these gases. As an upper limit we take the

Table 9: Momentum ranges, in GeV/ c , per particle for each PID with the addition of each detector.

Particle	TPC	TOF	+CKOV	+RICH
π	0.1-0.7	0.7-2.7	2.5-7.5	5-80
K	0.1-0.7	0.7-2.7	2.5-4.6	7.5-80
p	0.1-1.1	0.7-4.6	7.5-17.5	17-120

dispersion coefficients given in [18], which would lead to a contribution of 1 mm to σ_R in the case of Ne. This estimate gives momentum limits which are approximately half of those cited above for CO₂. More accurate calculations of the ring containment and dispersion effects will be performed shortly.

With this array of detectors the particle identification is nearly continuous, as shown in Fig. 32, and Table 9. Both the table and figure adopt a simplified pid scheme, where particles are considered to be identified by dE/dx or TOF only if their momentum is below the point where the 3σ bands begin to cross, by CKOV threshold if this additional information resolves the TOF ambiguity, and by RICH if the momentum is within threshold and below the 3σ crossing, or if its information resolves an earlier ambiguity. With the present experimental layout pions and kaons are not identified above 80 GeV/ c . Protons and kaons are not unambiguously identified between 4.6 and 7.5. In addition, the region around 1 GeV/ c has poor coverage.

5.4 Data Acquisition

P907's anticipated 100 Hz rate of minimum bias data allows for a rather simple data acquisition and trigger system. For most of the running it will be sufficient to require that some charged particles are produced and detected outside of the beam envelope. This trigger can be implemented using the TOF array as an indication of the charged particle multiplicity in conjunction with segmented counters near the target. Similar triggers have been implemented in BNL E910 and FNAL E690 and are very effective at obtaining minimum bias events. Standard FASTbus electronics available from Fermilab PREP can be used to digitize signals from all of the detector systems except for the TPC. The presenence of a minimum bias event trigger, and the absence of a "BUSY" initiates the digitization and readout. If more restrictive triggers are necessary or desirable, they can be formed during the digitization time and result in a "RESET" (the trigger calculation being false). The number of bytes per event is relatively small (50 to 100kBytes); the anticipated recording rate of 10 MBytes/sec is well within the state of the art in recording technologies.

To obtain the 100 Hz event rate modifications to the TPC data acquisition system must be implemented. In BNL E910 the maximum rate was 60 Hz, limited, in priciple, by the front end electronics. However, the actual data rates of 20 Hz resulted from the data acquisition system limitations. This limit can be overcome by using more modern computer and networking hardware and a more modern "event builder" architecture. This upgrade can be accomplished by a modest investment in computer hardware and software development.

PID Acceptance (positives)

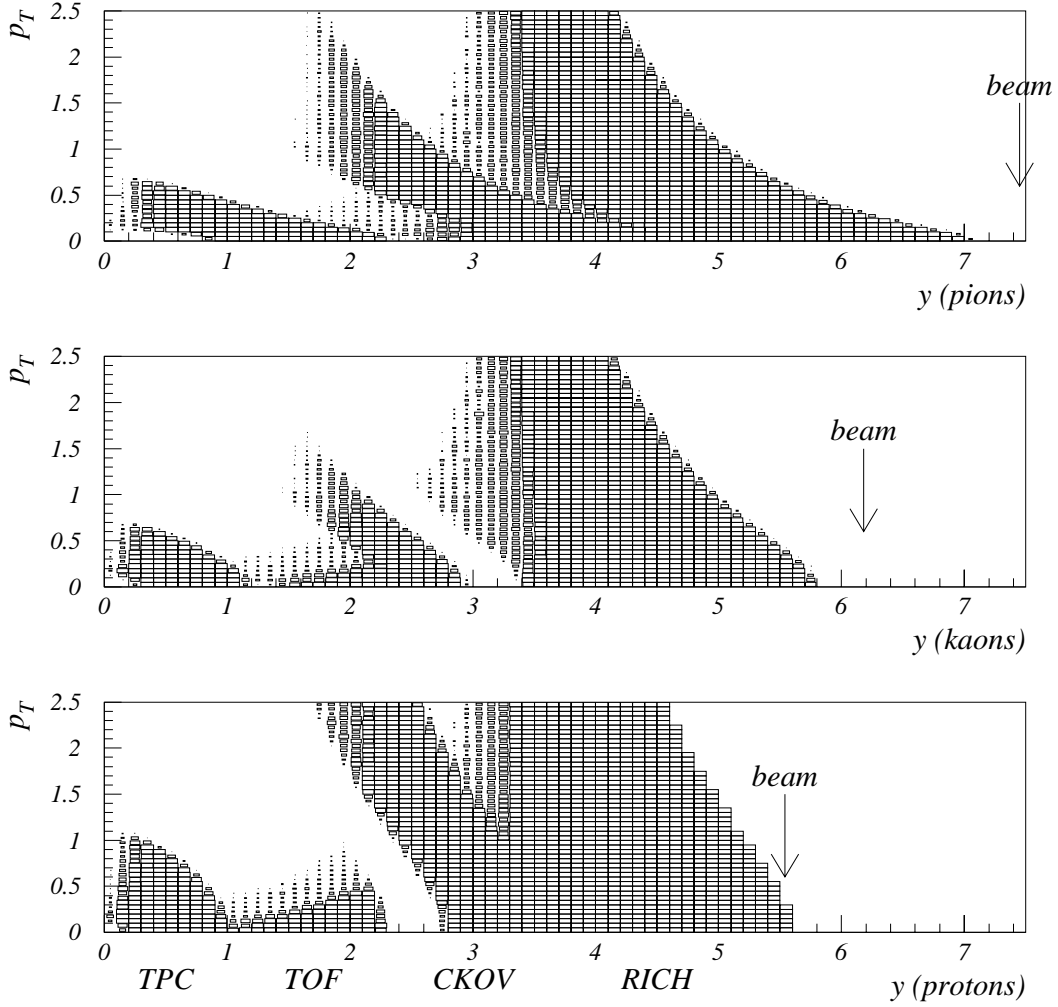


Figure 32: Particle identification acceptances for positive particles.

The limitations due to the front end electronics of the TPC require new developments. The factor of 2 increase in rate is modest, designs have been discussed but further developments await a demonstrated need and availability of resources.

6 Cost and Schedule

We have begun to develop a complete bottom-up cost and manpower estimate for P-907. By “complete,” we mean we have covered all systems and sub-systems of the experiment, including the upstream beamline. We have also included removal of existing equipment from Meson Center to make way for this experiment. The work breakdown structure (WBS) is shown with our cost estimate in Table 10.

On the manpower side, we have included physicist and engineering to complete the physics design, to plan and manage the installation, and to commission the detector. We have also made preliminary estimates of the number of physicists that will be required to operate the experiment during data running and to perform the basic analysis. The manpower estimates are important inputs in assessing the potential impact on MINOS of undertaking this experiment at Fermilab.

To date we have not made a detailed schedule. This will require greater understanding, on our part, of the detailed requirements for installing and operating each detector system, and guidance from Fermilab on the availability of engineering and technical personnel, and a likely target date for first beam.

In the remainder of this section we will discuss the scope of our estimate, our estimating method, contingency, and, finally, the scope and method used to estimate the manpower requirements.

6.1 Cost Estimate

6.1.1 Scope of Estimate

Almost all experiment systems are based on existing equipment. By using existing systems with proven performance we eliminate the detector research and development phase, drastically shortening the design cycle and reducing the experiment cost. The engineering and design process for these systems is largely limited to “infrastructure” issues: mounting, installing, connecting electrical and other services, and data cabling.

The trigger and DAQ designs, of necessity, must be specific to the experiment, however, they will be based on existing components and infrastructure, as discussed in Section 5.4. This will reduce to a minimum the design effort. Procurement costs will be largely limited to cables. The use of local (Nevis, FNAL DART) or commercial (FASTbus, VME) systems will facilitate the adoption and reuse of existing communications and control software.

At this time we have not located suitable existing detectors that could function as our time-of-flight (TOF) or neutral calorimeters (NCAL). As placeholders for these systems, we have included $\sim \$30\text{K}$ each, pending location of suitable existing systems.

Since we propose to run with both 120 GeV/c primary beam from the Main Injector, as well as 5–110 GeV/c secondary beams, the upstream beamline is not trivial. We have included in this estimate the costs associated with designing and constructing this beamline, based on the design discussed in Section 4.2, including the secondary beam production target, detectors to enable accurate targeting of Main Injector primary beam on the production target, a dispersive bend with adjustable aperture to make the momentum selection, beam species tagging using threshold Čerenkov counters, and tracking detectors to enable accurate

targeting of the beam onto the experimental target.

Meson Center was most recently used by E871 (Hyper-CP). A certain amount of disassembly and cleanout is required before P-907 can be installed. We have included a preliminary estimate for this work.

6.1.2 Estimate Methodology and Basis

Since most detector systems are based on existing hardware, most of the WBS items require a fairly detailed understanding of the component designs and infrastructure requirements to produce detailed designs for costing. Therefore, at this stage cost estimating has been limited to known costs of similar recent tasks, detailed below, and engineer or physicist estimates, generally at WBS level three.

For each task, we separately estimate the level of effort required from physicists, engineers, and technicians, and the materials and supplies. We use nominal Fermilab rates, including fringe benefits, for engineers and technicians, as provided by John Cooper. (Engineer II, \$352/day; Tech Specialist, \$284/day; Senior Tech, \$206/day; Tech II, \$174/day) We assume that physicist effort is not charged directly to the experiment, however the level of physicist effort required *is* part of the estimate (see the discussion of manpower, below). Engineers (and physicists) are counted as EDIA (engineering, design, inspection, and administration), technicians as labor. (Since physicists are assumed to be zero cost for the project, however, their efforts don't increase the totaled costs.)

Technician effort has been further broken out into "FNAL & E907", work that is most naturally staffed by Fermilab and/or the collaboration; and "FNAL | T&M", work that could be accomplished by T&M contracts, at approximately 2.5 times the cost. Despite the increased cost (\$37.4K increasing to \$93.5K), contracting this work through T&M might be desirable to reduce the workload on Fermilab staff by 36 man weeks.

Materials and supplies, M&S, is also broken down into T&M contracts for heavy rigging, and all other M&S, which are largely parts procurements.

Where possible, the estimates have been based on known effort and costs for similar tasks accomplished in the recent past. Tasks and costs for rigging and magnet connections/disconnections were developed with the generous assistance of Leon Beverly and Mike Mascione in PPD, based on recent work in MC6, MC8, and Lab G.

Before the last run of the Hyper-CP experiment, an access was made to the MC6SW magnet in the upstream section of the MC6 Target Pile. Opening just this section of the pile took a T&M rigging crew of five people one week, at an approximate cost of \$10k. This effort of five man weeks forms the basis for the estimates in WBS 2 and 3 for opening and closing the MC6 Pretarget Enclosure and Target Pile.

The rate for T&M rigging (\$500/man day) is based on the contract work completed in the last few months to remove the Jolly Green Giant and a second large magnet from Lab G, which required 3.5 crew weeks at a cost of \$42k. The effort in Lab G forms the basis for the estimate to reassemble the Jolly Green Giant and TPL-B magnets in the MC7 worm.

Table 10: Work breakdown structure (WBS) and preliminary cost estimates by task. For each task EDIA (engineering, design, inspection, and administration), Labor, M&S (materials and supplies) are rolled up separately. Labor is further broken down into “FNAL & E907”, labor to be provided by Fermilab and E907, or “FNAL | T&M”, labor that can be provided by Fermilab (to minimize cost) or by T&M contracts (to minimize the use of Fermilab manpower). We have assumed that this labor is provided by Fermilab. M&S is further broken down into “T&M”, contracts for heavy rigging, and “Other M&S” for the remainder. The last column shows the total cost for each task. We assume that physicist effort is not charged directly to the experiment; tasks with zero direct cost are to be done by physicists, as shown in the manpower estimate, below.

WBS	Task Name	EDIA	Labor	NAL & E907	FNAL T&M	M&S	T&M	Other M&S	Total Cost
0	Fermilab E907	\$138,160	\$295,894	258488	37406	\$536,100	277500	258600	\$970,154
1	Experiment Design	\$0	\$0	0	0	\$0	0	0	\$0
2	Meson Hall (MC6) Preparation	\$1,760	\$26,408	3480	22928	\$100,000	100000	0	\$128,168
2.1	MC6 Cleanout Planning	\$1,760	\$0	0	0	\$0	0	0	\$1,760
2.2	MC6 Clear Storage from Top of Piles	\$0	\$15,180	0	15180	\$0	0	0	\$15,180
2.3	Open and Clear Pretarget Enclosure (P)	\$0	\$9,520	2784	6736	\$50,000	50000	0	\$59,520
2.3.1	PTE Remove Concrete Lid Blocks	\$0	\$0	0	0	\$37,500	37500	0	\$37,500
2.3.2	PTE Remove Steel Lid	\$0	\$0	0	0	\$12,500	12500	0	\$12,500
2.3.3	PTE Remove Steel Side Walls	\$0	\$5,060	0	5060	\$0	0	0	\$5,060
2.3.4	PTE Disconnect Magnets	\$0	\$2,784	2784	0	\$0	0	0	\$2,784
2.3.5	PTE Remove Magnets	\$0	\$1,676	0	1676	\$0	0	0	\$1,676
2.4	Open and Clear Target Pile (TP)	\$0	\$1,708	696	1012	\$50,000	50000	0	\$51,708
2.4.1	TP Remove Concrete Lid Blocks	\$0	\$0	0	0	\$25,000	25000	0	\$25,000
2.4.2	TP Remove Steel Plugs	\$0	\$0	0	0	\$12,500	12500	0	\$12,500
2.4.3	TP Remove Downstream Concrete Bl	\$0	\$0	0	0	\$12,500	12500	0	\$12,500
2.4.4	TP Disconnect Magnet	\$0	\$696	696	0	\$0	0	0	\$696
2.4.5	TP Remove Magnet	\$0	\$1,012	0	1012	\$0	0	0	\$1,012
3	E907 Beamline (in MC6)	\$0	\$15,200	10140	5060	\$100,000	100000	0	\$115,200
3.1	Secondary Beamline (BEAM) Magnet In	\$0	\$10,140	10140	0	\$0	0	0	\$10,140
3.1.1	BEAM Install 3 Dipoles	\$0	\$6,180	6180	0	\$0	0	0	\$6,180
3.1.2	BEAM Install 4 Quadrupoles	\$0	\$2,060	2060	0	\$0	0	0	\$2,060
3.1.3	BEAM Survey	\$0	\$1,900	1900	0	\$0	0	0	\$1,900
3.2	Close Pretarget Enclosure	\$0	\$5,060	0	5060	\$50,000	50000	0	\$55,060
3.2.1	PTE Replace Steel Side Walls	\$0	\$5,060	0	5060	\$0	0	0	\$5,060
3.2.2	PTE Replace Steel Lid	\$0	\$0	0	0	\$12,500	12500	0	\$12,500
3.2.3	PTE Replace Concrete Lid Blocks	\$0	\$0	0	0	\$37,500	37500	0	\$37,500
3.3	Close Target Pile	\$0	\$0	0	0	\$50,000	50000	0	\$50,000
3.3.1	TP Replace Downstream Concrete Bl	\$0	\$0	0	0	\$12,500	12500	0	\$12,500
3.3.2	TP Replace Steel Plugs	\$0	\$0	0	0	\$12,500	12500	0	\$12,500
3.3.3	TP Replace Concrete Lid Blocks	\$0	\$0	0	0	\$25,000	25000	0	\$25,000
4	Meson Worm (MC7) Preparation	\$0	\$13,726	9056	4670	\$31,500	22500	9000	\$45,226
4.1	Remove or Stage Hyper-CP Detectors	\$0	\$4,560	4560	0	\$0	0	0	\$4,560
4.1.1	MC7 Stage 9 PWC	\$0	\$3,800	3800	0	\$0	0	0	\$3,800
4.1.2	MC7 Remove 2 HODO	\$0	\$760	760	0	\$0	0	0	\$760
4.2	Remove BM109 Magnets	\$0	\$5,526	2756	2770	\$22,500	22500	0	\$28,026
4.2.1	MC7 Disconnect BM109 Magnets	\$0	\$1,030	1030	0	\$0	0	0	\$1,030
4.2.2	MC7 Prep Outside Area for Crane	\$0	\$2,770	0	2770	\$0	0	0	\$2,770
4.2.3	MC7 Move Utilities	\$0	\$1,030	1030	0	\$0	0	0	\$1,030
4.2.4	MC7 Open Worm	\$0	\$696	696	0	\$0	0	0	\$696
4.2.5	MC7 Rig Out BM109 Magnets	\$0	\$0	0	0	\$22,500	22500	0	\$22,500
4.3	Close MC7 Worm	\$0	\$3,640	1740	1900	\$9,000	0	9000	\$12,640
4.3.1	MC7 Restore Utilities	\$0	\$1,740	1740	0	\$0	0	0	\$1,740
4.3.2	MC7 Replace Panels and Insulation	\$0	\$1,900	0	1900	\$9,000	0	9000	\$10,900

Table 10: (continued)

WBS	Task Name	EDIA	Labor	NAL & E907	FNAL T&M	M&S	T&M	Other M&S	Total Cost
5	E907 Experiment (in MC7)	\$136,400	\$240,560	235812	4748	\$304,600	55000	249600	\$681,560
5.1	Upstream Beamline Detectors (UBL)	\$7,040	\$26,780	26780	0	\$0	0	0	\$33,820
5.1.1	UBL Design	\$7,040	\$0	0	0	\$0	0	0	\$7,040
5.1.2	UBL Secondary Production Target Fa	\$0	\$8,240	8240	0	\$0	0	0	\$8,240
5.1.3	UBL Tracking Chamber Refurbishmen	\$0	\$4,120	4120	0	\$0	0	0	\$4,120
5.1.4	UBL Threshold Cerenkov (tCKV) Fabr	\$0	\$8,240	8240	0	\$0	0	0	\$8,240
5.1.5	UBL Installation	\$0	\$6,180	6180	0	\$0	0	0	\$6,180
5.1.5.1	UBL Pretarget Enclosure Detecto	\$0	\$4,120	4120	0	\$0	0	0	\$4,120
5.1.5.2	UBL Target Pile Detectors Installa	\$0	\$2,060	2060	0	\$0	0	0	\$2,060
5.2	Experimental Targets (ETGT)	\$12,320	\$20,600	20600	0	\$0	0	0	\$32,920
5.2.1	Target Wheel (TGTW)	\$1,760	\$3,090	3090	0	\$0	0	0	\$4,850
5.2.1.1	TGTW Design	\$1,760	\$0	0	0	\$0	0	0	\$1,760
5.2.1.2	TGTW Fabrication	\$0	\$2,060	2060	0	\$0	0	0	\$2,060
5.2.1.3	TGTW Installation	\$0	\$1,030	1030	0	\$0	0	0	\$1,030
5.2.2	Cryogenic Target (CTGT)	\$7,040	\$12,360	12360	0	\$0	0	0	\$19,400
5.2.2.1	CTGT Design	\$7,040	\$0	0	0	\$0	0	0	\$7,040
5.2.2.2	CTGT Fabrication	\$0	\$8,240	8240	0	\$0	0	0	\$8,240
5.2.2.3	CTGT Installation	\$0	\$4,120	4120	0	\$0	0	0	\$4,120
5.2.3	NuMI Target Sample (NTGT)	\$3,520	\$5,150	5150	0	\$0	0	0	\$8,670
5.2.3.1	NTGT Design	\$3,520	\$0	0	0	\$0	0	0	\$3,520
5.2.3.2	NTGT Fabrication	\$0	\$4,120	4120	0	\$0	0	0	\$4,120
5.2.3.3	NTGT Installation	\$0	\$1,030	1030	0	\$0	0	0	\$1,030
5.3	Target Recoil Detector (TRD)	\$28,160	\$24,720	24720	0	\$0	0	0	\$52,880
5.3.1	TRD Design	\$28,160	\$0	0	0	\$0	0	0	\$28,160
5.3.2	TRD Fabrication	\$0	\$12,360	12360	0	\$0	0	0	\$12,360
5.3.3	TRD Installation	\$0	\$12,360	12360	0	\$0	0	0	\$12,360
5.4	Time Projection Chamber (TPC)	\$10,560	\$16,962	16962	0	\$22,300	0	22300	\$49,822
5.4.1	TPC Move to FNAL	\$0	\$7,692	7692	0	\$12,300	0	12300	\$19,992
5.4.2	TPC Assess Condition	\$0	\$1,030	1030	0	\$0	0	0	\$1,030
5.4.3	TPC Installation Design	\$10,560	\$0	0	0	\$0	0	0	\$10,560
5.4.4	TPC Installation	\$0	\$8,240	8240	0	\$10,000	0	10000	\$18,240
5.5	Jolly Green Giant (JGG)	\$7,040	\$4,235	4235	0	\$85,000	25000	60000	\$96,275
5.5.1	JGG Move & Installation Design	\$7,040	\$0	0	0	\$0	0	0	\$7,040
5.5.2	JGG Replacement Coil	\$0	\$0	0	0	\$60,000	0	60000	\$60,000
5.5.3	JGG Assembly	\$0	\$0	0	0	\$25,000	25000	0	\$25,000
5.5.4	JGG Connections	\$0	\$4,235	4235	0	\$0	0	0	\$4,235
5.6	Differential Cerenkov (CKOV)	\$14,080	\$29,400	28292	1108	\$27,300	0	27300	\$70,780
5.6.1	CKOV Move & Installation Design	\$7,040	\$0	0	0	\$0	0	0	\$7,040
5.6.2	CKOV Move	\$0	\$7,692	7692	0	\$2,300	0	2300	\$9,992
5.6.3	CKOV Undercarriage Fabrication	\$3,520	\$8,240	8240	0	\$10,000	0	10000	\$21,760
5.6.4	CKOV Freon Recovery Fabrication	\$3,520	\$8,240	8240	0	\$10,000	0	10000	\$21,760
5.6.5	CKOV Locate in Position	\$0	\$1,108	0	1108	\$0	0	0	\$1,108
5.6.6	CKOV Connections	\$0	\$4,120	4120	0	\$5,000	0	5000	\$9,120
5.7	Time-of-Flight (TOF)	\$10,560	\$16,480	16480	0	\$0	0	0	\$27,040
5.7.1	TOF Design	\$10,560	\$0	0	0	\$0	0	0	\$10,560
5.7.2	TOF Fabrication	\$0	\$8,240	8240	0	\$0	0	0	\$8,240
5.7.3	TOF Installation	\$0	\$8,240	8240	0	\$0	0	0	\$8,240
5.8	TPL-B Magnet (TPL-B)	\$7,040	\$4,235	4235	0	\$25,000	25000	0	\$36,275
5.8.1	TPL-B Move & Installation Design	\$7,040	\$0	0	0	\$0	0	0	\$7,040
5.8.2	TPL-B Assembly	\$0	\$0	0	0	\$25,000	25000	0	\$25,000
5.8.3	TPL-B Connections	\$0	\$4,235	4235	0	\$0	0	0	\$4,235
5.9	Ring Imaging Cerenkov (RICH)	\$9,680	\$30,198	26557	3640	\$45,000	5000	40000	\$84,878
5.9.1	RICH Move & Installation Design	\$7,040	\$0	0	0	\$0	0	0	\$7,040
5.9.2	RICH Extraction from PC4	\$880	\$12,626	11170	1456	\$5,000	5000	0	\$18,506
5.9.2.1	RICH Downstream Flange Stan	\$880	\$2,930	2930	0	\$0	0	0	\$3,810
5.9.2.1.1	RICH D/S Flange Stand Desi	\$880	\$1,030	1030	0	\$0	0	0	\$1,910
5.9.2.1.2	RICH D/S Flange Stand Fabr	\$0	\$1,900	1900	0	\$0	0	0	\$1,900
5.9.2.2	RICH Remove PMTs	\$0	\$4,120	4120	0	\$0	0	0	\$4,120
5.9.2.3	RICH Open End Flanges	\$0	\$1,456	0	1456	\$0	0	0	\$1,456
5.9.2.4	RICH Remove Mirrors	\$0	\$2,060	2060	0	\$0	0	0	\$2,060
5.9.2.5	RICH Disconnect Support Equipm	\$0	\$2,060	2060	0	\$0	0	0	\$2,060
5.9.2.6	RICH Lift Components Through P	\$0	\$0	0	0	\$5,000	5000	0	\$5,000
5.9.3	RICH New Tank	\$1,760	\$0	0	0	\$40,000	0	40000	\$41,760
5.9.4	RICH Position New Tank in MC7	\$0	\$728	0	728	\$0	0	0	\$728
5.9.5	RICH Install Mirrors	\$0	\$1,998	1997	0	\$0	0	0	\$1,998
5.9.6	RICH Close End Flanges	\$0	\$1,456	0	1456	\$0	0	0	\$1,456
5.9.7	RICH Install Support Equipment	\$0	\$4,120	4120	0	\$0	0	0	\$4,120
5.9.8	RICH Gas Clean & Fill	\$0	\$1,030	1030	0	\$0	0	0	\$1,030
5.9.9	RICH Install PMTs	\$0	\$4,120	4120	0	\$0	0	0	\$4,120
5.9.10	RICH Install Electronics	\$0	\$4,120	4120	0	\$0	0	0	\$4,120

Table 10: (continued)

WBS	Task Name	EDIA	Labor	NAL & E907	FNAL T&M	M&S	T&M	Other M&S	Total Cost
5.10	Drift Chambers (DC)	\$5,280	\$31,930	31930	0	\$100,000	0	100000	\$137,210
5.10.1	DC Move & Installation Design	\$5,280	\$3,090	3090	0	\$0	0	0	\$8,370
5.10.2	DC Move	\$0	\$8,240	8240	0	\$0	0	0	\$8,240
5.10.3	DC Parts Fabrication	\$0	\$12,360	12360	0	\$100,000	0	100000	\$112,360
5.10.4	DC Installation	\$0	\$8,240	8240	0	\$0	0	0	\$8,240
5.11	Neutral Hadron Calorimeter (NCAL)	\$10,560	\$16,480	16480	0	\$0	0	0	\$27,040
5.11.1	NCAL Design	\$10,560	\$0	0	0	\$0	0	0	\$10,560
5.11.2	NCAL Fabrication	\$0	\$8,240	8240	0	\$0	0	0	\$8,240
5.11.3	NCAL Installation	\$0	\$8,240	8240	0	\$0	0	0	\$8,240
5.12	Trigger (TRG)	\$7,040	\$6,180	6180	0	\$0	0	0	\$13,220
5.12.1	TRG Design	\$7,040	\$0	0	0	\$0	0	0	\$7,040
5.12.2	TRG Fabrication	\$0	\$4,120	4120	0	\$0	0	0	\$4,120
5.12.3	TRG Installation	\$0	\$2,060	2060	0	\$0	0	0	\$2,060
5.13	Data Acquisition (DAQ)	\$7,040	\$12,360	12360	0	\$0	0	0	\$19,400
5.13.1	DAQ Design	\$7,040	\$0	0	0	\$0	0	0	\$7,040
5.13.2	DAQ Fabrication	\$0	\$8,240	8240	0	\$0	0	0	\$8,240
5.13.3	DAQ Installation	\$0	\$4,120	4120	0	\$0	0	0	\$4,120
6	Data Taking (DATA)	\$0	\$0	0	0	\$0	0	0	\$0
6.1	DATA Engineering Run	\$0	\$0	0	0	\$0	0	0	\$0
6.2	DATA 1% Targets	\$0	\$0	0	0	\$0	0	0	\$0
6.3	DATA NuMI Target Running	\$0	\$0	0	0	\$0	0	0	\$0
7	Core Analysis	\$0	\$0	0	0	\$0	0	0	\$0
7.1	Analysis Development	\$0	\$0	0	0	\$0	0	0	\$0
7.1.1	UBL Analysis Development	\$0	\$0	0	0	\$0	0	0	\$0
7.1.2	TRD Analysis Development	\$0	\$0	0	0	\$0	0	0	\$0
7.1.3	TPC Analysis Development	\$0	\$0	0	0	\$0	0	0	\$0
7.1.4	JGG Analysis Development	\$0	\$0	0	0	\$0	0	0	\$0
7.1.5	CKOV Analysis Development	\$0	\$0	0	0	\$0	0	0	\$0
7.1.6	TOF Analysis Development	\$0	\$0	0	0	\$0	0	0	\$0
7.1.7	TPL-B Analysis Development	\$0	\$0	0	0	\$0	0	0	\$0
7.1.8	RICH Analysis Development	\$0	\$0	0	0	\$0	0	0	\$0
7.1.9	DC Analysis Development	\$0	\$0	0	0	\$0	0	0	\$0
7.1.10	NCAL Analysis Development	\$0	\$0	0	0	\$0	0	0	\$0
7.1.11	TRG/DAQ Analysis Development	\$0	\$0	0	0	\$0	0	0	\$0
7.2	Tracking & PID Integration	\$0	\$0	0	0	\$0	0	0	\$0
7.2.1	UBL-TGT-TRD-TPC Tracking	\$0	\$0	0	0	\$0	0	0	\$0
7.2.2	TPC-CKOV Tracking & PID	\$0	\$0	0	0	\$0	0	0	\$0
7.2.3	CKOV-TOF Tracking & PID	\$0	\$0	0	0	\$0	0	0	\$0
7.2.4	TOF-RICH Tracking & PID	\$0	\$0	0	0	\$0	0	0	\$0
7.2.5	RICH-NCAL Tracking	\$0	\$0	0	0	\$0	0	0	\$0
7.3	Core Analysis Production	\$0	\$0	0	0	\$0	0	0	\$0
8	Project Management	\$0	\$0	0	0	\$0	0	0	\$0

The Jolly Green Giant magnet has a short in one of the coils that developed when it was moved from Brookhaven to Fermilab circa 1990 for E690. Despite considerable detective work, the E690 experimenters were unable to discover who built the coil originally when (the now defunct) Allis Chalmers built the magnet for the CEA. In 1991 the E690 experimenters obtained a budgetary quote of \$55K, to build a replacement coil, from Pacific Electric Motor, the likely source of the original coil. (Based on the limited diagnostic information available, PEM expressed the opinion that there was a high probability that the coil could be repaired, at one tenth to one quarter the cost.) Since that time, escalation of approximately 30% should be partially offset by the decrease in the price of copper, also approximately 30%. For this proposal we have used \$60K as the procurement cost for a new coil.

The costs of opening and closing the MC7 worm roof to enable crane access for the magnet assembly are based on the actual costs incurred in opening and closing the MC8 worm roof to extract steel shielding blocks.

The effort to extract the RICH was estimated by Mike Mascione, who was the supervisor when it was installed in PC4. For the RICH we examined two options: retrieving all components of the existing RICH; or retrieving everything except for the tank, and purchasing

a new tank. The main difficulty in retrieving the tank is moving it into position under the access hatch, which is at the downstream end of PC4. When the tank was installed, before the downstream detectors, access was not an issue. Now, however, there are approximately six detector systems and copious stored material in the way. We have identified a sequence of moves that will bring the tank under the hatch to be lifted out. However, this sequence requires moving the intervening detectors more than the service loops will allow. This will necessitate cutting many cable bundles with little regard for any potential future uses for the detectors. Retrieving the tank will also use approximately 13 additional man weeks of Fermilab labor. Finally, our coarse cost estimates indicate that retrieving the tank will cost approximately \$15K more than constructing a new tank. This savings depends critically on the cost of a new tank, however, which we have based on escalation of the original price from circa 1993, as provided by Jim Kilmer. It would be prudent, therefore, to make the final decision on the basis of a firm bid for a new tank. The existing tank has the advantage that it is known to be leak tight, whereas fabricating a new tank introduces the risks of shaking down a new component.

At this time we have no firm funding commitments from any source, so no “credits” have been taken. Fermilab funding and rates have been assumed. However, one of our collaborating institutions (Livermore) has expressed interest in supporting some of the construction and/or operation expenses, in addition to contributing physicist effort. Such support could be “in kind” and/or through funds transfer. This possibility is contingent on the scope of their own internal funding, and will almost certainly require negotiations on the part of the spokesman and Fermilab resulting in an MOU between the laboratories. If this contribution is realized, a separate rollup of costs by laboratory will likely be required.

6.1.3 Contingency

Because of the very limited level of detail available at this early stage in the design, the confidence interval on the cost estimate must be somewhat broad. Certainly any contingency estimate less than 35–50% is unjustified at this stage. Since most of the tasks are fairly narrow in scope, however, completion of the design tasks should result in fairly good cost and effort estimates for the actual work.

As a reference point, we can look at the partial dismantlement of the Meson Polarized target piles (MP6) in the Meson Hall. This work resulted in \$60K of captured costs, and approximately \$10–20K of uncaptured labor effort, according to Paul Czarpatha and Harlan Dick. A direct comparison is difficult since the scope of work was different. The MP6 work involved partial (semi-destructive) dismantlement of the pile, including special procedures and handling to address contamination issues, and installation of the recovered steel as shielding in the Booster area. (The scope of work in MC6 is unlikely to disturb lower sections of the piles containing most of the contamination.) Approximately half of the material in the MP6 pile was removed, over a length approximately half of the MC pile length. Roughly speaking, then, opening the MC pile should cost double the MP6 cost. The rollup for WBS 2, Meson hall (MC6) Preparation, is \$125K, roughly double the MP6 dismantlement cost, as expected. Similarly, relacing the shielding in MC6 after configuring our beamline is approximately equal to the estimate for removing the shielding.

The comparison to the work done in MP6 provides some confidence that our estimates

for the beamline work (WBS 2 and 3) are not off by a large factor. Similarly, the very recent work to remove magnets from Lab G provides a sound basis for estimating the magnet assembly costs in MP7 (WBS 5.4 and 5.7). These items only account for 35% of the cost, however, leaving a substantial fraction of the total cost with a larger uncertainty.

6.2 Manpower Estimate

As a necessary part of developing the cost estimate, we have estimated the level of physicist, engineer, and technician effort required to design, install, commission, operate, and analyse the experiment. Beyond the cost estimate, the central issue for us is to assess the likely impact on MINOS of mounting this experiment at Fermilab in the near future.

To examine this issue, we have taken a number of steps in preparing the estimate. First, we have estimated the engineering effort by discipline, mechanical or electrical. Second, we have separated engineering and technician effort, since these will likely be impacted at different times in the schedule for this experiment (as well as for MINOS). Third, we have included physicist effort, in order to understand the size of collaboration required.

We have done a physicist estimate of the level of physicist effort required for each task. We have assigned two physicists half time for six months to finalize the experiment design. Generally we have included a physicist at one-quarter time for the duration of each system design task. Exceptions are the time-of-flight and neutral calorimeter, where, since no existing system has been identified, we have assigned a full physicist. For the TPC assessment we have assigned four physicists for a week. For the trigger and DAQ we have assigned a full time physicist.

During the operation of the experiment, we assume a total of 16 physicists will be required to cover 24 hour per day running with beam.

The manpower estimate is shown in Table 11. In man years, the totals amount to approximately 12 physicist years, 1.5 engineer years (split equally between mechanical and electrical), and 5.5 technician years.

6.2.1 Physicist Effort for Core Analysis

Finally, we have taken the somewhat unusual step of estimating the physicist effort involved in producing a bare minimum analysis, comprising acceptance determination, quantification of systematic errors, and determination of particle type and relativistic four-vectors for all observed particles. These outputs are the common core that all further physics analyses will be based on, yet involve no specializations for any particular topic.

For example, the set of four-vectors measured off the sample MINOS (NuMI) target are sufficient input for a simple MINOS beam simulation, based directly on the observed particle production. The set of four-vectors are also the input to phenomenological parametrizations, such as Malensek [51].

Production and distribution of the core analysis output will make it possible for interested physicists to pursue further a topic of their choice. At the same time, the core analysis output is the minimum data product required to enable the accurate determination of neutrino spectrum and beam composition required by MINOS.

Table 11: Work breakdown structure (WBS) rolled up by effort for Physicists, Engineers, and Technicians, in man weeks.

WBS	Task Name	Physicist	Engineer	Technician
0	Fermilab E907	573.9	78.5	280.65
1	Experiment Design	39	0	0
2	Meson Hall (MC6) Preparation	0	1	26.6
3	E907 Beamline (in MC6)	1	0	15
4	Meson Worm (MC7) Preparation	0	0	14.6
5	E907 Experiment (in MC7)	88.9	77.5	224.45
5.1	Upstream Beamline Detectors (UBL)	5	4	26
5.2	Experimental Targets (ETGT)	1.75	7	20
5.3	Target Recoil Detector (TRD)	16	16	24
5.4	Time Projection Chamber (TPC)	9	6	11
5.5	Jolly Green Giant (JGG)	1	4	4.5
5.6	Differential Čerenkov (CKOV)	1.4	8	23.2
5.7	Time-of-Flight (TOF)	8	6	16
5.8	TPL-B Magnet (TPL-B)	1	4	4.5
5.9	Ring Imaging Čerenkov (RICH)	6.25	5.5	30.25
5.10	Drift Chambers (DC)	1.5	3	31
5.11	Neutral Hadron Calorimeter (NCAL)	4	6	16
5.12	Trigger (TRG)	10	4	6
5.13	Data Acquisition (DAQ)	24	4	12
6	Data Taking (DATA)	288	0	0
6.1	DATA Engineering Run	32	0	0
6.2	DATA 1% Targets	224	0	0
6.3	DATA NuMI Target Running	32	0	0
7	Core Analysis	144	0	0
7.1	Analysis Development	96	0	0
7.2	Tracking & PID Integration	40	0	0
7.3	Core Analysis Production	8	0	0
8	Project Management	13	0	0

As a zero'th order estimate, we have assumed that two man-months of effort will be required to develop the analysis for each detector system (upstream beamline, target recoil detector, Jolly Green Giant field, differential Čerenkov, time-of-flight, TPL-B field, RICH, drift chamber tracking, neutral calorimeter, trigger and DAQ) and four man-months to develop the TPC analysis. In addition, we have assumed that two man-months of effort will be required to match up the tracking and particle identification at each “interface” (upstream beamline, target, target recoil detector, and TPC; TPC and Čerenkov; Čerenkov and time-of-flight; time-of-flight and RICH; and RICH and neutral calorimeter). Finally, we have assumed two man-months for the core analysis production pass on all data.

A Schedule for 120 GeV Beam to the Meson Lab

The Switchyard 120 GeV project (SY120) is an Accelerator Improvement Project (AIP) approved by DOE and funded over a four year period to revise the beams extracted to the Meson Lab and KaMI to be suitable for the needs of transporting 120 GeV beams to expected experiments. The principal revisions are replacement of cryogenic magnet strings with conventional magnets and the addition of quadrupoles to contain the larger beam within the existing apertures.

Given the revised funding profile of the project, including the expected shortfall of money in FY2001, the present schedule for availability of beam to the Meson Lab is as follows. In January 2001 it will be possible to send 120 GeV beams to Meson Center and Meson Test at low intensity (of order 10^{11} protons per cycle), without the addition of the new quadrupoles and without the installation of the secondary beam elements necessary for the less-than 120 GeV goals of P-907.

In FY2002, the schedule calls for adding the necessary quadrupoles, moving the Meson three way split to a more appropriate location in view of the larger beam sizes, and installing the secondary beam for P-907. The secondary beam for P-907, and small revisions to get the beam to Meson Test, are included in this AIP project.

C. Thornton Murphy
Project Leader, SY120

References

- [1] G. Rai *et al.*, *IEEE Trans. Nucl. Sci.* **37**, 56 (1990); LBL-28141
- [2] J. Engelfried *et al.* *Nucl. Instr. and Meth.* **A431**, 53 (1999); FERMILAB-PUB-98-299-E.
- [3] “P-875: A long baseline neutrino oscillation experiment at Fermilab”, MINOS Collaboration, E. Ables *et al.*; FERMILAB-PROPOSAL-P-875, (1995).
- [4] “HARP- Proposal to study hadron production for the neutrino factory and for the atmospheric neutrino flux”, M.G. Catanesi *et al.*, CERN-SPSC/99-35.
- [5] “Status and future programme of the NA49 Experiment”, M. Botje *et al.*, CERN/SPSC/2000-011.
- [6] N. V. Mokhov *et al.*, Fermilab-Conf-98/379 (1998); LANL Report LA-UR-98-5716 (1998); *nucl-th/9812038 v2 16 Dec 1998*; <http://www-ap.fnl.gov/MARS/>.
- [7] See <http://wwwinfo.cern.ch/asd/geant/index.html> for GEANT User’s guide, CERN, unpublished
- [8] N.V. Mokhov and S.I. Striganov FERMILAB-CONF-98-53 (1998).
- [9] N.I. Bozhko *et al.*, *Sov. J. Nucl. Phys.* **31**, 775 (1980); *Sov. J. Nucl. Phys.* **29**, 345 (1979) - $67\text{ GeV}/c$.
- [10] H.W. Atherton *et al.* CERN 80-07 - $400\text{ GeV}/c$.
- [11] G. Ambrosini *et al.*, *Eur. Phys. Jour. C* **10**, 605 (1999) - $450\text{ GeV}/c$.
- [12] L.M. Barkov *et al.*, *Z. Phys.* **14**, 1 (1982); L.M. Barkov *et al.*, *Sov. J. Nucl. Phys.* **37**, 732 (1983) - $70\text{ GeV}/c$.
- [13] NA44 collaboration, H. Boggild *et al.* *Phys. Rev. C* **59**, 328 (1999) - $450\text{ GeV}/c$.
- [14] D.S. Barton *et al.*, *Phys. Rev. D* **27**, 2580 (1983) - $100\text{ GeV}/c$.
- [15] R.Raja, *Phys. Rev. D* **18**, 204 (1978).
- [16] R.Raja, *Phys. Rev. D* **16**, 142 (1977). This paper describes an original formula derived by the spokesman in estimating the annihilation component in $\bar{p}p$ interactions
- [17] R.Raja, Y.Fisyak in Proceedings of the DPF92 meeting, Fermilab.
- [18] J. Litt and R. Meunier, *Ann. Rev. Nucl.Sci.* **23**, 1 (1973).
- [19] J.F. Donoghue, E. Golowich, B.R. Holstein, “Dynamics of the Standard Model”, p. 275 *ff*, Cambridge University Press (1992).
- [20] Particle Data Group, “Review of Particle Physics”, *Phys. Rev. D* **54**, 1–720 (1996).

- [21] K. Goulianos, *Phys. Rep.* **101**, 169 (1973).
- [22] Kyriacos Markianos, “Spin Parity Measurement of Centrally Produced ($\pi^+\pi^-$) in Proton-Proton Collisions at 800 GeV/c”, UMAHEP 449, University of Massachusetts, Amherst 1997, thesis, *unpublished*.
- [23] T. Abbott *et al.* *Phys. Rev. D*, **45**, 3906 (1992).
- [24] K. Abe *et al.* *Phys. Lett.* **200**, 266 (1988).
- [25] E. Andersen *et al.* *Phys. Lett. B*, **433**, 209 (1998).
- [26] H. Bialkowska *et al.* *Z. Phys. C*, **55**, 491 (1992).
- [27] J.D. Bjorken. *Phys. Rev. D*, **27**, 140 (1983).
- [28] W. Busza *et al.* *Phys. Rev. Lett.*, **34**, 836 (1975).
- [29] W. Busza and A.S. Goldhaber. *Phys. Lett. B*, **139**, (1984).
- [30] W. Busza and R.J. Ledoux. *Ann. Rev. Nucl. Part. Sci.*, **38** (1988).
- [31] I. Chemakin *et al.* *submitted to Phys. Rev. Lett.*, (1999); nucl-ex/9902009.
- [32] I. Chemakin *et al.* *Phys. Rev. C* **60**, 024902 (1999).
- [33] I. Chemakin *et al.* *submitted to Phys. Rev. Lett.* (2000); nucl-ex/0003010.
- [34] T.K. Choi *et al.* *Phys. Rev. C* **55**, 848 (1997).
- [35] B.A. Cole and X. Yang, 2000. Private communication.
- [36] J.E. Elias *et al.* *Phys. Rev. D*, 22:13, 1980.
- [37] European Organization for Nuclear Research. Press release, feb. 10, 2000. <http://press.web.cern.ch/Press/Releases00/PR01.00EquarkGluonMatter.html>.
- [38] M. Gazdzicki and D. Rohrich. *Z. Phys. C* **71**, 55 (1996).
- [39] W.S. Toothacker *et al.* *Phys. Lett.*, **197**, 295 (1987).
- [40] “Centrality dependence of strangeness production in proton-nucleus collisions at AGS energies”, X. Yang. PhD thesis, Columbia University, 2000.
- [41] J.D. Bjorken, *Acta Phys. Pol. B*, **23**, 637 (1992) and references therein.
- [42] Y.Fukuda *et al.* (SuperKamiokande Collaboration), *Phys. Rev. Lett.* **81**, 1562 (1998).
- [43] T.Kajita, *Nucl. Phys.* **B77**, 123 (1999).
- [44] H.W. Atherton *et al.*, CERN report number CERN 80-07 (1980).

- [45] G. Ambrosini *et al.*, *Phys. Lett. B*, **420**, 225 (1998); G.Ambrosini *et al.*, *Phys. Lett. B*, **425**, 208 (1998); G.Ambrosini *et al.*, *Eur. Phys. J. C*, **10**, 605 (1999).
- [46] See <http://www.fnal.gov/projects/muon-collider/nu-factory/> for the Fermilab neutrino factory feasibility study.;
- [47] B. Autin *et al.* “Physics opportunities at a CERN based neutrino factory”, CERN-SPSC-98-30, Oct 1998;
- [48] “The MINOS Detectors Technical Design Report”, NuMI-L-337.
- [49] C.L. Wang, *Phys. Rev. D* **10**, 3876 (1974).
- [50] G. Cocconi *et al.*, LBL Report No. UCRL 10022, (1961).
- [51] A.J. Malensek, “Empirical Formula for Thick Target Particle Production”, Fermilab FN-341, October 12, 1981.
- [52] “Long baseline study of the leading neutrino oscillation at a neutrino factory”, V.Barger, S.Geer, R.Raja and K.Whisnant, *to be published in Phys Rev D*. (2000); hep-ph/9911524.
- [53] D. C. Christian *et al.*, *Nucl. Instr. and Meth.* **A345**, 62 (1994).
- [54] “The NuMI Facility Technical Design Report”, Revision 1.0, October, 1998, Fermilab
- [55] Private Communication, J. Engelfried
- [56] *Nucl. Phys.*, **A638**, 423c (1998).